Varicella-Zoster Virus ORF9 Is an Antagonist of the DNA Sensor cGAS

Jonny Hertzog[1], Rachel E. Rigby[1], Sonja Roll[1], Chiara Cursi[1], Lise Chauveau[1], Tamara Davenne[1], and Jan Rehwinkel[1,*]

[1]MRC Human Immunology Unit, MRC Weatherall Institute of Molecular Medicine, Radcliffe Department of Medicine, University of Oxford, Oxford, UK

*correspondence: jan.rehwinkel@imm.ox.ac.uk

ABSTRACT

Varicella-Zoster virus (VZV) causes chickenpox and shingles. Although infection is associated with severe morbidity in some individuals, the molecular mechanisms that determine innate immune responses remain poorly defined. We found that the cGAS/STING DNA sensing pathway was critically required for type I interferon (IFN) induction in response to VZV infection. Viral gene overexpression screening identified the essential VZV tegument protein ORF9 as a novel antagonist of DNA sensing via cGAS. Ectopically as well as virally expressed ORF9 bound to endogenous cGAS. Confocal microscopy revealed co-localisation of cGAS and ORF9, which blocked the type I IFN response to transfected DNA. ORF9 and cGAS also interacted directly in a cell-free system. Our data further suggest that ORF9 inhibited the production of cGAMP by cGAS. Taken together, our work highlights the importance of the cGAS/STING DNA sensing pathway for VZV recognition and identified an immune antagonist encoded by VZV that directly interferes with DNA sensing *via* cGAS.

INTRODUCTION

Varicella-Zoster virus (VZV) is one of nine herpes viruses that infect humans (Arvin and Gilden, 2013). VZV is an alpha-herpesvirus, closely related to Herpes Simplex virus (HSV) 1 and 2. It has a 125kb dsDNA genome, the smallest of the human herpesviruses. The genome includes at least 70 open reading frames (ORFs). Primary infection causes chickenpox (*Varicella*). Like all human herpes viruses, VZV establishes life-long latency in an infected host and can reactivate as shingles (*Zoster*). Shingles is a debilitating disease with significant associated morbidity. During both primary infection and reactivation, the virus can gain access to the central nervous system and cause severe complications such as encephalitis and vasculitis (Nagel and Gilden, 2014). Despite introduction of the live-attenuated chickenpox vaccine in the early 1990s, the virus remains highly prevalent worldwide (WHO, 2014).

The type I IFN system lies at the forefront of host defence against infectious pathogens and is indispensable for successful control of viral infections (McNab et al., 2015). The expression of these cytokines is induced following pattern recognition receptor (PRR) activation. PRRs are a heterogenous group of proteins that can respond to a diverse array of pathogen-associated molecular patterns (PAMPs) (Brubaker et al., 2015). The recognition of viral pathogens relies to a large extent on sensing of nucleic acids (Barrat et al., 2016; Hartmann, 2017). Both endosomal toll-like receptors and dedicated cytosolic sensors are potently activated by viral RNA and DNA. The DNA sensor cyclic GMP-AMP synthase (cGAS) synthesises the second messenger 2'3'-cyclic GMP-AMP (hereafter simply cGAMP), a cyclic di-nucleotide, upon direct binding to dsDNA (Ablasser et al., 2013; Sun et al., 2013; Wu et al., 2013). Binding of cGAMP to stimulator of IFN genes (STING) results in the activation of the transcription factors IRF3 and NFκB via the kinases TBK1 and IKKε (de Oliveira Mann et al., 2019; Diner et al., 2013; Fitzgerald et al., 2003; Ishikawa et al., 2009; Liu et al., 2015; Sharma et al., 2003; Zhang et al., 2019; Zhang et al., 2013) . Both transcription factors are responsible for the expression of IFNβ and other type I and type III IFNs, as well as inflammatory cytokines. Other proteins, such as IFI16, RNA polymerase III, and DNA-PK have been described to be accessory proteins to the cGAS/STING system or constitute independent DNA-sensing mechanisms (Dempsey and Bowie, 2015).

Type I IFNs are secreted cytokines that act in an autocrine, paracrine, or systemic manner by binding to the type I IFN receptor (IFNAR) (McNab et al., 2015). Canonical IFNAR signalling results in the phosphorylation and heterodimerisation of the transcription factors STAT1 and STAT2. After recruitment of IRF9, this protein complex drives expression of hundreds of genes, termed interferon-stimulated genes (ISGs). Among others, ISGs contain genes that encode PRRs, proteins involved in type I IFN induction and signalling, negative and positive feedback regulators, restriction factors acting directly on viruses, and proteins that are involved in adaptive immune responses (Schoggins, 2019; Schoggins et al., 2011).

Despite the fact that VZV is a highly prevalent and important human pathogen, its pathogenesis is still poorly understood. The lack of suitable small animal models that recapitulate primary infection and latency establishment has hampered the molecular

characterisation of its life cycle *in vivo* (Haberthur and Messaoudi, 2013). During its dissemination in the human host, the virus infects a multitude of different cells. Infection of T cells, keratinocytes, neurons, and epithelial cells is indispensable for VZV's life cycle (Zerboni et al., 2014). In addition, immune cells including dendritic cells (DCs), monocytes, and NK cells are capable of supporting VZV replication *in vitro* and are potentially relevant for *in vivo* spread (Abendroth et al., 2001; Campbell et al., 2018; Kennedy et al., 2019; Morrow et al., 2003; Wang et al., 2005). However, the events that govern the cell-intrinsic recognition of the virus in these cell types and the antiviral cytokine response have only begun to be elucidated *in vitro*. The DNA sensor TLR9 is partly responsible for IFNα secretion after infection of plasmacytoid DCs (Yu et al., 2011). In dermal fibroblasts, STING is required for type I and type III IFN production (Kim et al., 2017). An interesting genetic link between DNA sensing *via* RNA polymerase III and VZV CNS infection has been uncovered recently (Carter-Timofte et al., 2018). Although a comprehensive characterisation of the role of these DNA sensing pathways during VZV infection is lacking, current evidence suggests that type I IFNs are of critical relevance for control of VZV infection. Increased IFNα levels can be detected in the serum of patients with primary VZV infection (Arvin et al., 1986). In addition, the potency of type I IFNs in restriction of VZV replication has been demonstrated *in vitro* (Kim et al., 2017; Ku et al., 2016; Shakya et al., 2019; Torigo et al., 2000).

In this study we addressed the question which nucleic acid sensors induce type I IFN expression in response to VZV infection. We show that the cGAS - STING - TBK1 - IRF3 signalling axis was responsible for antiviral cytokine expression after VZV infection. We further report the generation of a VZV ORF expression library and identification of a viral cGAS antagonist. The tegument protein encoded by ORF9 blocked activation of cGAS and subsequent synthesis of cGAMP. Mechanistically, we show that ORF9 interacted with cGAS, likely by binding to DNA. We propose a model in which cGAS activation upon VZV infection is prevented immediately after viral entry through the tegument protein ORF9.

RESULTS

A Model System for VZV Infection

To identify PRRs that induce type I IFN in response to VZV infection we chose to use the monocytic cell line THP1. We hypothesised a role of DNA sensors in VZV infection given its identity as a DNA virus and the previously shown role of STING in recognition of VZV (Kim et al., 2017). THP1 cells, unlike many other immortalised cell lines, induce type I and type III IFNs *via* cGAS in response to DNA (Sun et al., 2013; Wu et al., 2013). Furthermore, THP1 cells are amenable to genome editing and knockout (KO) lines can be used to genetically dissect the role of individual proteins involved in pattern recognition. THP1 cells are permissive for VZV infection and propagation (Nour et al., 2011) and VZV infects primary human monocytes and macrophages *in vitro* and *in vivo* (Kennedy et al., 2019; Mainka et al., 1998). In addition to wild-type (WT) THP1 cells, we tested previously described KO lines lacking cGAS, STING, TBK1, MyD88, or IFNAR2. We further generated MAVS KO and IRF3 KO cells using CRISPR/Cas9 technology (see Materials and Methods and Figure S1). All THP1 KO cells were validated by immunoblotting for the absence of protein and functionally by stimulation with DNA, RNA and type I IFN (Figure S2).

Upon treatment with PMA, THP1 cells adopt a macrophage-like, adherent and highly responsive phenotype. Given the difficulties of working with cell-free VZV (Caunt and Taylor-Robinson, 2009; Chen et al., 2004), we used co-culture with VZV-infected (+VZV) MeWo cells to infect PMA-treated THP1 cells; co-culture with uninfected MeWo cells served as a control (Figure S3A). MeWo cells are a melanoma cell line that is well-established for VZV propagation. After 48 hours of co-culture, cells were harvested for RT-qPCR, immunoblotting, and flow cytometry analysis. Before co-culturing, THP1 cells were labelled with a fluorescent tracer dye to distinguish inoculum (MeWo) and target (THP1) cells during flow cytometry analysis (Figure S3A,B). For all experiments, uninfected MeWo cells were additionally used as target cells. MeWo cells do not induce type I IFNs in response to VZV (Figure 1). Infected cells within the target cell population were identified by cell-surface staining for the VZV glycoprotein E (gE)/glycoprotein I (gI) complex (Figure S3B) (Mo et al., 2003).

Due to the nature of the co-culture, cells harvested for RT-qPCR and immunoblotting contained both target and inoculum cells. Flow cytometry analysis revealed that across genotypes, target cells constituted between 50% and 85% of all cells in uninfected samples and between 70% and 95% in infected samples (Figure S3C). Amongst target cells, the infected cell population constituted between 10% and 30% of cells (Figure S3D). This showed that all THP1 KO cell lines tested here were permissive for VZV infection.

The Type I IFN Response to VZV Requires the DNA Sensor cGAS

To investigate whether THP1 cells induce type I IFNs in response to VZV we analysed mRNA expression levels of *IFNB1* (encodes IFNβ) and *IFI44*, an ISG. In WT THP1 cells, both transcripts were robustly induced after VZV infection (Figure 1A). Similar results were obtained using MyD88 KO and MAVS KO cells. In contrast, no

transcriptional upregulation of *IFNB1* or *IFI44* was observed in THP1 cells lacking cGAS, STING, TBK1, IRF3, or IFNAR2.

Immunoblot analysis showed that the transcription factors STAT1 and STAT2 were only phosphorylated in WT, MyD88 KO, and MAVS KO cells (Figure 1B). In contrast, no p-STAT1 and p-STAT2 signals were observed in cells lacking cGAS, STING, TBK1, IRF3, or IFNAR2. This indicated that only WT, MyD88 KO and MAVS KO cells secreted type I IFNs in response to VZV infection. Consistently, STAT1 and RIG-I, which are both encoded by ISGs, were upregulated at protein level only in the cells showing STAT1/2 activation (Figure 1B). Importantly, we could not observe phosphorylation of STAT1/2 or increased abundance of STAT1 and RIG-I in infected MeWo cells. Western blotting with antibodies against VZV-gE/gI and VZV ORF62 confirmed that all cell lines became infected.

Determination of CXCL10 (IP-10) levels in co-culture supernatants confirmed the findings of our RT-qPCR and immunoblot analyses. WT, MyD88 KO, and MAVS KO THP1 cells produced low levels of CXCL10 at baseline and these were increased after infection with VZV (Figure 1C). No CXCL10 was detected in supernatants from uninfected and infected cGAS KO, STING KO, TBK1 KO, and IFNAR2 KO THP1 cells; similarly, MeWo cells did not secrete CXCL10. We could detect low levels of CXCL10 in supernatants from IRF3 KO cells but there was no increase above baseline after infection. Collectively these results demonstrate that in THP1 cells the type I IFN response to VZV infection required the DNA sensor cGAS and the STING – TBK1 – IRF3 signalling axis. It is therefore likely that dsDNA is the PAMP recognised in VZV-infected cells.

A VZV ORF Expression Library

Type I IFNs inhibit VZV infection (Kim et al., 2017; Ku et al., 2016). VZV, like many other viruses, employs immune evasion strategies that target the type I IFN system. For example, both ORF61 and ORF62 prevent IRF3 activation through distinct mechanisms (Sen et al., 2010; Zhu et al., 2011). In light of our finding that cGAS was crucial for type I IFN induction in response to VZV, we hypothesised that the virus expresses a direct antagonist of cGAS and/or STING. Indeed, other large DNA viruses often encode multiple antagonists of the same innate immune pathway (Smith et al., 2018; Stempel et al., 2019). In order to test the role of individual viral gene products in immune evasion we generated an expression library for all canonical VZV ORFs. All coding sequences were PCR-amplified and cloned into a gateway entry vector. Using recombination, these sequences were then shuttled into a lentiviral vector (pLenti6.3/TO/V5). This vector allows expression with a C-terminal V5 epitope tag either after transient transfection or *via* lentiviral transduction. To validate these constructs, we transiently transfected HEK293T cells and analysed expression of VZV proteins by immunoblot using an antibody against the V5-tag (Figure S4). 59 of 72 constructs (82%) were expressed and bands at the expected molecular weights were detected. Five constructs were expressed but at the wrong size, and eight were not expressed at all. This VZV ORF library is a resource for the scientific community and is available to all interested scientists.

Identification of ORF9 as an Antagonist of DNA sensing

To investigate whether VZV ORFs block cGAS/STING activation, we utilised a luciferase-based screening platform in HEK293T cells. In brief, a plasmid expressing Firefly luciferase under *IFNB1* promotor control and pRL-TK, which constitutively expresses Renilla luciferase, were transiently transfected. HEK293T cells do not express cGAS and STING naturally. We therefore reconstituted human cGAS and human STING by transient transfection, which results in activation of the *IFNB1* promotor and firefly luciferase expression. Lastly, individual viral ORFs (or controls) were co-expressed. Firefly luciferase expression was normalised to Renilla luciferase expression, and we calculated for each ORF a luciferase fold change to an empty vector control condition without cGAS and STING expression constructs. The mean and standard deviation of all data points was then used to calculate Z-values, which represent the number of standard deviations an individual data point is diverging from the mean. We used these Z-scores to rank ORFs in their ability to block IFN activation downstream of cGAS/STING (Figure 2A). KSHV ORF52, a previously described cGAS-antagonist (Wu et al., 2015), and the L protein of EMCV, a previously described IRF3-antagonist (Freundt et al., 2018), served as positive controls. As expected, we found these with the lowest ranks (i.e. smallest fold change) in our assay and both potently blocked firefly luciferase induction. In addition, we identified a number of VZV ORFs that showed similar behaviour. The two aforementioned IRF3 antagonists expressed by VZV, ORF61 and ORF62, were among them, which further validated our approach.

We performed this screening experiment three times; Figure 2B displays the results as a heatmap. We identified a number of ORFs that reproducibly ranked very low. To identify VZV proteins that specifically block the cGAS and/or STING, and not downstream signalling proteins such as IRF3 that are also activated by other PRRs, we compared selected hits from the primary screen in their ability to block reporter activation by overexpression of cGAS/STING or RIG-I-CARD (data not shown). RIG-I-CARD is a constitutively active variant of RIG-I that activates the *IFNB1* promotor *via* MAVS. A direct cGAS/STING antagonist is therefore unable to block this stimulation. We identified the protein encoded by ORF9 of VZV to selectively block reporter activation by cGAS/STING but not RIG-I-CARD when compared to empty vector (Figure 2C).

We then aimed to verify that VZV ORF9 has the ability to antagonise activation of cGAS by dsDNA in an endogenous setting. THP1 monocytes were stably transduced with expression constructs for ORF9-V5 or for GFP-V5 as a negative control (Figure 2D). We stimulated cGAS in these cells by transfection of increasing doses of dsDNA and measured expression levels of *IFNB1* mRNA and *IFNL1* mRNA (encoding a type III IFN) by RT-qPCR (Figure 2E). As expected, THP1 cells expressing GFP showed a dose-dependent increase in expression of both transcripts. In contrast, cells expressing ORF9 did not respond to low doses of DNA. At higher doses, their response was attenuated when compared to GFP-expressing cells. Collectively, these data revealed that the VZV ORF9 protein prevented cGAS/STING activation.

VZV ORF9 Interacts With cGAS

We hypothesised that VZV ORF9 exerts its antagonistic function by directly interacting with either cGAS or STING. To test this, HEK293T cells were transiently transfected with expression constructs for cGAS-FLAG, STING-HA, and ORF9-V5 and protein interaction was analysed by immunoprecipitation (IP). We used antibodies against the epitope tags and analysed IP fractions by immunoblotting (Figure 3A). All ectopically expressed proteins were precipitated efficiently, and an IgG isotype control antibody did not precipitate any of the proteins tested. Interestingly, ORF9 was detected in the bound fraction after cGAS IP. The reverse IP confirmed this result: we found cGAS in the ORF9 IP. In contrast, ORF9 did not interact with STING in this assay (Figure 3A). To verify that this interaction occurred with endogenous cGAS, we used THP1 cells stably transduced to express FLAG-ORF9, which was precipitated from cell lysates with α-FLAG antibody. Indeed, endogenous cGAS was present in the IP fraction; IP of FLAG-GFP served as a negative control (Figure 3B).

Next, we asked whether ORF9 expressed from its endogenous promotor during viral infection had the ability to interact with cGAS. We used a recombinant VZV that expressed C-terminally V5-tagged ORF9 from its endogenous genomic locus. We infected THP1 cells and HaCaT cells (a keratinocyte cell line that expresses cGAS) with WT VZV or VZV$^{ORF9\text{-}V5}$ and performed α-V5 IP (Figure 3C). In both THP1 and HaCaT cells infected with VZV$^{ORF9\text{-}V5}$, endogenous cGAS co-precipitated with ORF9. These data showed that endogenous ORF9 protein expressed by the virus in infected cells interacted with cGAS.

To investigate whether the two proteins interact in living cells, we overexpressed tagged ORF9 and cGAS in HEK293T cells and performed immunofluorescence analysis (Figure 3D). Expression of ORF9 alone resulted in cytoplasmic staining. Similarly, cGAS was detected in the cytoplasm. We further observed cGAS foci co-localising with extranuclear DNA. Extranuclear DNA foci, sometimes in the form of micronuclei, can be observed in some cancer cells and have been shown to bind cGAS (Harding et al., 2017; Hu et al., 2019; Mackenzie et al., 2017). Interestingly, when ORF9 and cGAS were expressed together, both proteins co-localised in DAPI-positive, extranuclear regions. This indicated that ORF9 interacted with cGAS in cells and localised together with cGAS in DNA-positive areas.

In order to biochemically characterise the interaction between ORF9 and cGAS in more detail, we performed experiments in a cell-free system. We expressed cGAS, cGAS-HA, FLAG-ORF9, and FLAG-GFP in *E. coli* and performed single-step purification (Figure S5). First, we tested whether ORF9 and cGAS interacted directly using the far western protocol (Figure 3E). FLAG-ORF9 or FLAG-GFP protein were separated on a denaturing SDS-PAGE gel and transferred to a membrane. The proteins on the membrane were then re-natured and incubated with recombinant cGAS as a probe. Possible binding of cGAS to proteins on the membrane was then tested using α-cGAS antibody. Indeed, we found that probing for cGAS resulted in a signal at the size of ORF9 (Figure 3F). Importantly, cGAS did not bind to GFP.

We then tested interaction of the two recombinant proteins using immunoprecipitation. FLAG-ORF9 or FLAG-GFP were incubated with cGAS-HA in the test tube. The

proteins were then precipitated using antibodies against the epitope tags. Immunoblot analysis of the IP fractions showed that cGAS was co-immunoprecipitated with ORF9 but not GFP (Figure 3G). The reverse IP of cGAS resulted in binding of both ORF9 and GFP; however, the signal was stronger for ORF9. These data established that VZV ORF9 and cGAS interacted without the requirement for another cellular or viral protein.

To gain insight into possible structural features of ORF9 we used the PSIPRED 4.0 algorithm to predict its secondary structure based on the amino acid sequence (Buchan and Jones, 2019). This analysis predicted a four sheet - helix motif in the N-terminal region and a two helix - sheet - helix motif in the C-terminal region of ORF9 (Figure 4A). Using six ORF9 truncation mutants (Figure 4A), we tested whether these putative structural elements were involved in the interaction with cGAS. Firstly, we overexpressed both human cGAS and ORF9 mutants in HEK293T cells. Consistent with our earlier observation, full-length ORF9 co-immunoprecipitated cGAS. The C-terminal half of ORF9 (construct II) behaved the same, while the N-terminal half (construct I) failed to interact with cGAS. ORF9 constructs III, IV, and V also pulled down cGAS. All ORF9 constructs that interacted with cGAS shared amino acids (AA) 151 to 240. Interestingly, this region harbours the predicted two helix - sheet - helix motif. However, IP of ORF9$^{151\text{-}240}$ (construct VI) did not co-precipitate cGAS (Figure 4B). Secondly, we tested whether endogenous cGAS interacted with selected ORF9 truncation mutants stably expressed in THP1 cells. Consistent with the data from HEK293T cells, we found that full-length ORF9 and constructs II and V interacted with endogenous cGAS, while constructs I and VI did not (Figure 4C). Taken together, these biochemical and imaging data established that VZV ORF9 and cGAS were interaction partners. Furthermore, our results suggested that the central portion of ORF9 (construct VI, AA 151-240) was required but not sufficient for this interaction. However, it is also possible that ORF9$^{151\text{-}240}$ does not fold correctly in isolation.

ORF9 binds DNA

We next considered how ORF9 might block DNA sensing by cGAS and hypothesised that ORF9 binds DNA. We incubated biotinylated VACV-70mer dsDNA with recombinant ORF9; recombinant cGAS and GFP served as positive and negative controls, respectively. The VACV-70mer is a well-established immunostimulatory dsDNA that binds cGAS (Almine et al., 2017; Lum et al., 2018; Unterholzner et al., 2010). The DNA was then precipitated using streptavidin beads and the presence of bound proteins was analysed by immunoblotting (Figure 4D). In the absence of DNA, none of the proteins were precipitated. As expected, cGAS bound to DNA. Interestingly, ORF9 also was pulled down by DNA, both alone and in the presence of cGAS. GFP did not bind DNA under any conditions. These data show that ORF9 bound DNA, which may be related to its activity as a cGAS antagonist.

VZV ORF9 Prevents cGAMP Synthesis

cGAS activation by dsDNA results in the synthesis of cGAMP. Given our findings that ORF9 blocked DNA sensing and interacted with cGAS and DNA, we next tested

whether ORF9 prevents cGAMP production. Transfection of HEK293T cells with plasmids encoding GFP-tagged HIV-1 gag and VSV-G results in the production of VSV-G pseudotyped, HIV-1 GFP-capsid containing virus-like particles (VLPs). Co-expression of cGAS during VLP production leads to the presence of cGAMP within the particles (Bridgeman et al., 2015; Chauveau et al., 2020). We hypothesised that the presence of ORF9 during VLP production blocks cGAS activation and thus prevents the presence of cGAMP in VLPs. We produced VLPs in the presence or absence of cGAS with additional co-transfection of ORF9, or GFP as a negative control (Figure 5A). VLP producer cells were analysed by immunoblotting (Figure 5B). Infection of HEK293 cells and quantification of GFP-positive cells by flow cytometry confirmed equivalent infectivity of the different VLP preparations (Figure 5C, S6). The HEK293 cells used in this assay endogenously express STING. In response to cGAMP present in VLPs, these cells produce type I IFN, which we measured using a bioassay (Bridgeman et al., 2015; Chauveau et al., 2020). As expected, no type I IFN could be detected in response to infection with VLPs produced in the absence of cGAS (Figure 5D). In contrast, particles produced in the presence of cGAS and GFP potently stimulated type I IFN production. The presence of ORF9 during particle production with cGAS completely abrogated type I IFN stimulatory activity. This observation indicates that ORF9 prevented cGAMP production by cGAS.

DISCUSSION

VZV is a highly prevalent human pathogen, yet little is known for this virus about host-pathogen interactions and innate immunity. Here we report that cGAS and its downstream signalling pathway consisting of STING, TBK1 and IRF3 were required for type I IFN induction after VZV infection. An earlier study using RNA interference had implicated STING in innate recognition of VZV (Kim et al., 2017). Our results confirm this observation by complete genetic ablation, and – importantly – identify cGAS as the DNA sensor for VZV. It is possible that innate sensing pathways that detect VZV differ between cell types. Indeed, a study using inhibitory oligonucleotides found that plasmacytoid DCs produce type I IFN in a partially TLR9-dependent manner (Yu et al., 2011). In contrast, we found that the essential TLR9 adaptor protein MyD88 was dispensable for type I IFN induction in VZV infected THP1 cells. It will be interesting to characterise innate sensing pathways in different cell types relevant to *in vivo* infection, including neuronal cells, T cells and skin cells. This is important because the viral life cycle and effects of viral replication on host cells can differ between cell types (Zerboni et al., 2014). For example, VZV shows cytopathic effects in fibroblast and some immune cells but does not induce cell death in neurons (Gerada et al., 2020). Future investigation should therefore not only address the role of PRRs in induction of cytokines such as type I IFNs but also of cell death.

Our identification of cGAS as a sensor of VZV infection implicates recognition of an immunostimulatory DNA in infected cells. Studies of herpesvirus entry suggest that the viral DNA remains within the viral capsid during nuclear targeting and may therefore be unavailable for binding to cGAS (Radtke et al., 2006). Recently, single-cell analysis of HSV-1 infection showed that only cells undergoing abortive infection respond by production of type I IFNs (Drayman et al., 2019). It is therefore possible that viral particles with defective capsids are responsible for the type I IFN response observed in bulk populations of cells. Furthermore, cellular restriction mechanisms may make viral DNA from capsids accessible for cGAS binding. Indeed, degradation of herpesviral capsids *via* the ubiquitin – proteasome system has been suggested to release viral DNA for recognition (Horan et al., 2013). Alternatively, cellular DNA may induce type I IFN. Indeed, infections with multiple different viruses result in the accumulation of extranuclear DNA and in mitochondrial damage (Ablasser and Chen, 2019). Host DNA has been shown to stimulate cGAS in the context of HSV-1 infection (West et al., 2015). Whether viral and/or cellular DNA species activate cGAS in VZV-infected cells should be tested in the future by deep sequencing of cGAS-bound DNA. However, this approach has thus far been hampered by the lack of suitable antibodies for specific cGAS IP.

We further describe the identification of ORF9 as a cGAS antagonist. ORF9 interacted with cGAS in a variety of assays, and blocked cGAMP production and DNA-triggered type I IFN induction. ORF9 is a tegument protein, making it an attractive candidate for antagonising innate immunity. Tegument proteins are contained within viral particles and are delivered into cells at the same time as viral DNA. ORF9 may therefore prevent DNA sensing during early infection before viral gene expression. We speculate that

ORF9 exerts its function by disrupting cGAS-DNA interactions. Formation of multimeric complexes and higher order structures of cGAS and DNA facilitate cGAS activation (Andreeva et al., 2017; Du and Chen, 2018; Li et al., 2013; Zhang et al., 2014; Zhou et al., 2018). We show that ORF9 binds DNA, which may prevent formation of cGAS multimers (Andreeva et al., 2017). It is possible that ORF9 simply outcompetes cGAS by binding to DNA. However, we favour a model in which direct protein-protein interactions between the ORF9 and cGAS, as well as ORF9 – DNA interactions may prevent cGAS from forming higher order complexes. Future experiments will be required to decipher in detail the relationships between ORF9, cGAS, DNA, and cGAMP production. This should include testing the DNA length required for this given that cGAS oligomer formation is critically dependent on DNA length (Andreeva et al., 2017; Li et al., 2013; Luecke et al., 2017; Zhou et al., 2018).

ORF9 is essential for viral replication and is a member of the α-herpesvirus UL49 gene family (Che et al., 2008; Tischer et al., 2007). With its closest relative, HSV-1 VP22, it shares 36% AA sequence similarity (Hew et al., 2015). ORF9 has well-established roles in VZV nuclear egress and secondary envelopment (Che et al., 2013; Lebrun et al., 2018; Riva et al., 2013; Riva et al., 2015). Mutational analyses have attributed these functions to amino acids or regions either in the N-terminal half or the extreme C-terminus of the protein, whilst we describe a central region (AA151-240) to be required for the interaction of ORF9 with cGAS. A crystal structure is available for the core domain of HSV-1 VP22 that is homologous to this region of ORF9 (Hew et al., 2015). The HSV-1 VP22 core folds into a two helix - sheet - helix confirmation. Hew et al. further describe structural similarity between HSV1 VP22 and the unrelated MHV68 ORF52 (Hew et al., 2015). MHV68 ORF52 is the homologue of KSHV ORF52. Secondary structure prediction and examination of the published crystal structures revealed that VZV ORF9, HSV1 VP22, KSHV ORF52, and MHV68 ORF52 all potentially share a two helix – sheet structural feature (Figure S7). Interestingly, both HSV-1 VP22 and KSHV ORF52 have been described previously to inhibit cGAS activation (Huang et al., 2018; Wu et al., 2015). Antagonism of cGAS by KSHV ORF52 required its DNA binding properties. Collectively, these observations lead us to put forward a model in which distantly related herpesviruses have retained within unrelated proteins a structural feature that confers cGAS antagonist properties. Alpha, beta, and gamma-herpesviruses have been estimated to have evolutionarily diverged hundreds of millions of years ago (Brito and Pinney, 2018; Davison, 2002; McGeoch et al., 1995). Anemone species that have diverged from humans more than 500 million years ago harbour cGAS-like enzymes (Kranzusch et al., 2015). This indicates that a common ancestral organism expressed such proteins. It further opens up the possibility that ancient herpes viruses evolved the relevant evasion strategies. We hypothesise that antagonism of cGAS by herpesviruses constitutes an ancient molecular mechanism that evolved long before the advent of antiviral cytokines and IRF3 during evolution.

AUTHOR CONTRIBUTIONS

JH, RER and JR conceived the study, designed experiments and analysed data. JH, SR, CC, LC and TD performed experiments. JH and RER developed methodology. JH and JR wrote the manuscript. All authors read and approved the final manuscript.

ACKNOWLEDGMENTS

The authors thank J Cohen, C Sadzot and S Paludan for VZV stocks, antibodies and cell lines, and P Hublitz and Z Holloway (MRC WIMM Genome Engineering Facility) for their help with CRISPR plasmid generation. The authors further thank C Reis e Sousa, F Zhu, G Ogg, L Unterholzner, A Pichlmair, G Towers, T Fujita, J Haas, and M Reijns for reagents and advice. The authors thank M Brinkmann, J McKeating, and members of the Rehwinkel lab for critical discussion.

FUNDING

This work was funded by the UK Medical Research Council [MRC core funding of the MRC Human Immunology Unit] and by the Wellcome Trust [grant number 100954]. JH was supported by the European Commission under the Horizon2020 program H2020 MSCA-ITN GA 675278 EDGE. The MRC WIMM Genome Engineering Facility is supported by grants from the MRC/MHU (MC_UU_12009), the John Fell Fund (123/737) and by MRC WIMM Strategic Alliance awards G0902418 and MC_UU_12025. The funders had no role in study design, data collection and analysis, decision to publish, or preparation of the manuscript.

CONFLICT OF INTEREST

The authors declare no conflict of interest.

FIGURES

Figure 1

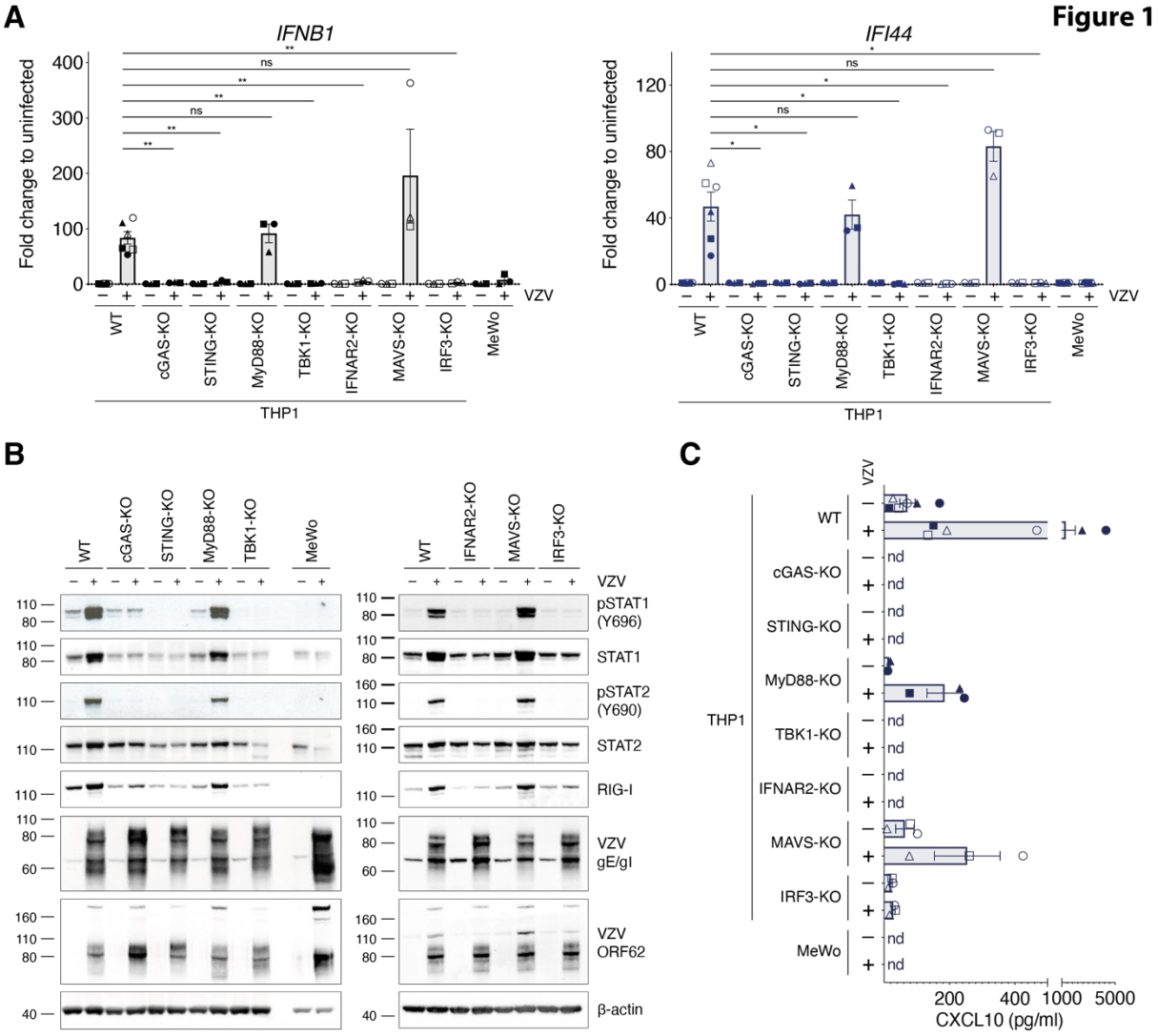

Figure 1. The cGAS/STING DNA sensing pathway induces type I IFNs in response to VZV infection.
(A) THP1 cells of the indicated genotypes were mock infected or infected with VZV by co-culture as described in Figure S3. The mRNA expression levels of *IFNB1* (encoding IFNβ) and *IFI44* were analysed by RT-qPCR. Expression levels were normalised to *GAPDH* and are shown as fold changes relative to levels in uninfected cells. **(B)** Cells were infected as in (A) and were analysed by western blot using the indicated antibodies. **(C)** Levels of CXCL10 (IP-10) in co-culture supernatants were quantified by ELISA.
Panels (A) and (C) show pooled data from six (THP1 WT, MeWo) or three (THP1 KOs) independent biological repeats (n=3/6 ± SEM). The different shapes of data points correspond to independent biological repeat experiments. Panel (B) shows a representative result of three independent repeats. Statistical analysis in panel (A) was one-way ANOVA with Dunnett's multiple comparisons test. **=p<0.01, *=p<0.05, ns=not significant.

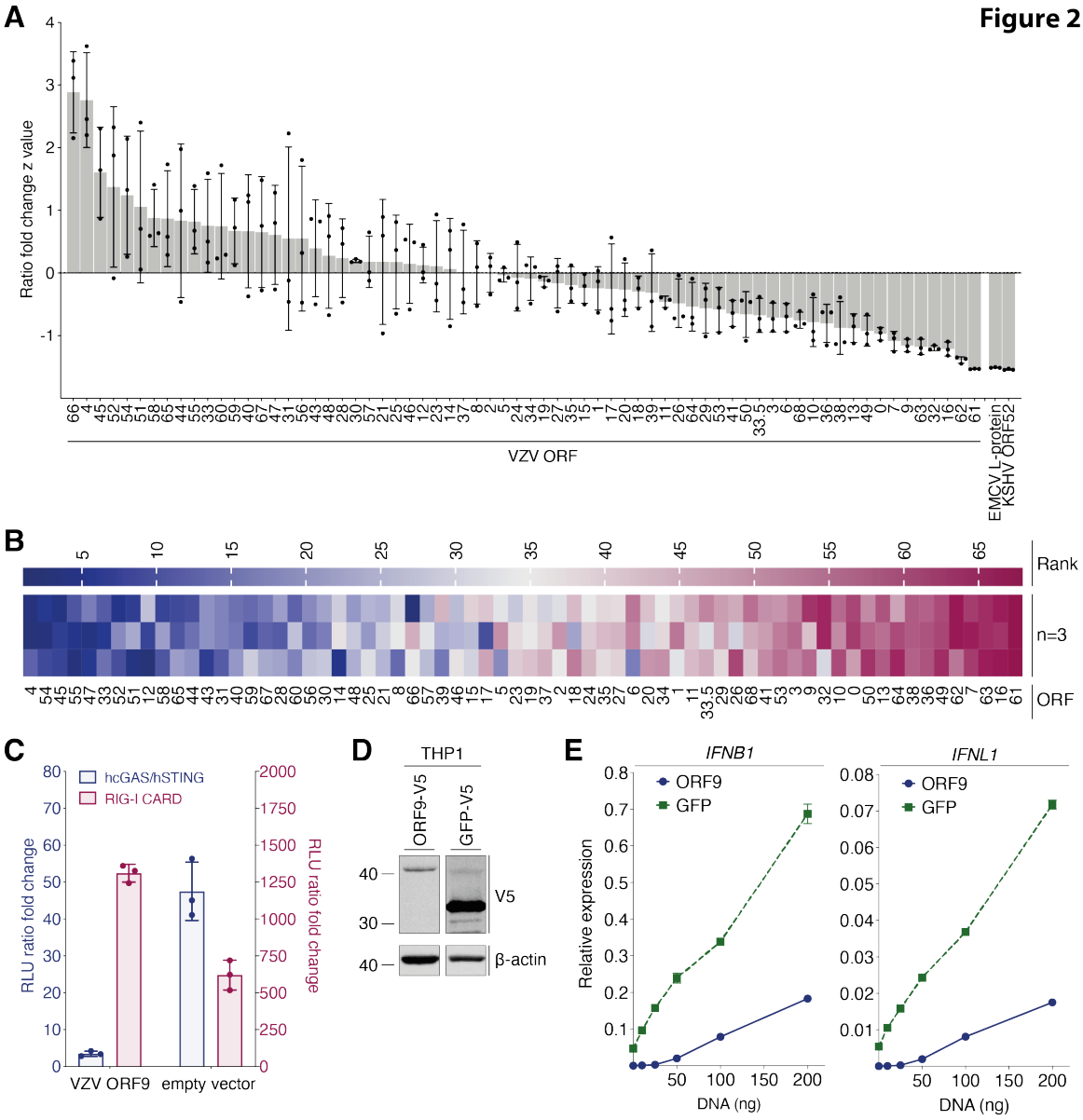

Figure 2. Screening of all VZV ORFs identifies ORF9 as an antagonist of cGAS-mediated DNA sensing.
(A) HEK293T cells were transfected with p125-F-Luc, pRL-TK, expression plasmids for human cGAS and human STING, as well as expression plasmids for individual VZV ORFs. The next day luciferase activity was determined. For each ORF a Z-value was calculated and ORFs were sorted in descending order. **(B)** The experiment shown in (A) was repeated three times and for each ORF in each experiment a rank was determined (highest Z-value = rank 1). Ranks are displayed as a heatmap. The order of the ORFs in the heatmap was determined by their average rank. **(C)** HEK293T cells were transfected as in (A) with expression constructs for VZV ORF9 or empty vector. In parallel, reporter expression was stimulated by co-transfection of the RIG-I-CARD plasmid instead of hcGAS and hSTING. A luciferase fold change was calculated to unstimulated cells. **(D)** Immunoblot analysis of THP1 cells stably transduced with either VZV ORF9-V5 or GFP-V5. **(E)** The same cells as in (D) were PMA-differentiated and transfected with the indicated doses of dsDNA. Expression of *IFNB1* and *IFNL1* mRNAs was assessed by RT-qPCR. Graphs show expression relative to *GAPDH*.
Panel (A) is representative of three independent experiments, which are summarised in panel (B). Panels (C) and (D) are representative of two independent experiments. Data points are technical triplicates with mean and standard deviation (A, C) or the average of technical duplicates with range (D).

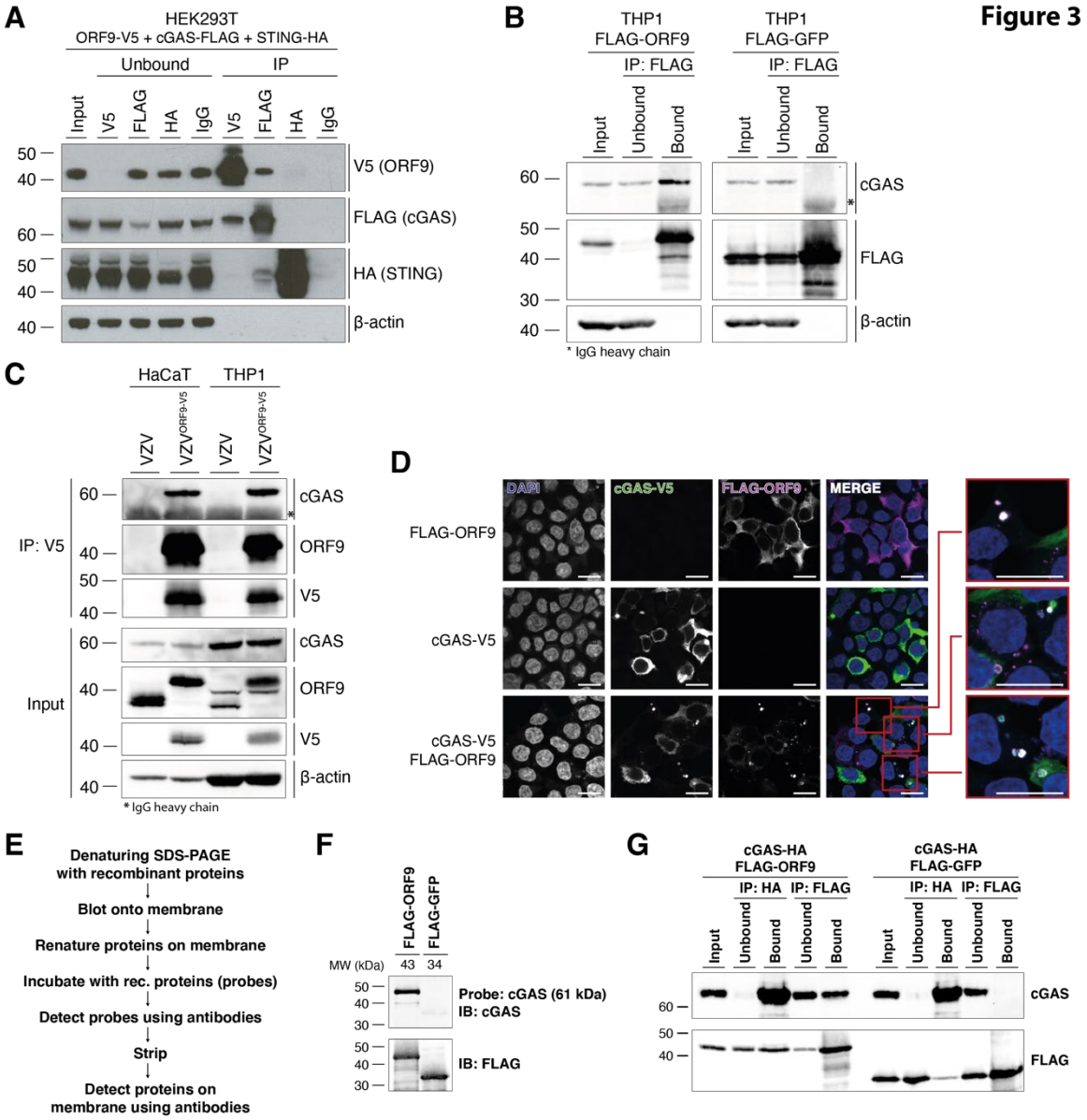

Figure 3. ORF9 interacts with cGAS.

(A) HEK293T cells were transfected with expression plasmids for ORF9-V5, human cGAS-FLAG, and human STING-HA. The next day, cells were lysed and overexpressed proteins were immunoprecipitated with α-V5, α-FLAG, α-HA, or IgG isotype control antibody. Input, unbound and IP fractions were subjected to immunoblotting using the indicated antibodies. **(B)** THP1 monocytes stably transduced with either VZV FLAG-ORF9 or FLAG-GFP were PMA-differentiated overnight. The next day, cells were lysed and ectopically expressed proteins were immunoprecipitated using α-FLAG antibody. Input, unbound and IP fractions were subjected to immunoblotting using the indicated antibodies. **(C)** HaCaT cells and PMA-differentiated THP1 cells were infected with WT VZV or $VZV^{ORF9\text{-}V5}$ through co-culture with infected MeWo cells for 48 hours. Cells were lysed and ORF9 was immunoprecipitated using α-V5 antibody. Input and IP fractions were subjected to immunoblotting using the indicated antibodies. **(D)** HEK293T cells were seeded onto glass coverslips and were transfected with human cGAS-V5, FLAG-ORF9, or both together. The next day, cells were fixed, permeabilised and stained using α-V5-FITC, rabbit-α-FLAG, and goat-α-rabbit-AF647 antibodies, and DAPI. Mounted coverslips were imaged using confocal microscopy. Scale bars: 15μm. **(E)** Outline of the far western protocol. **(F)** Far western analysis of cGAS-ORF9 interaction. Recombinant FLAG-ORF9 and FLAG-GFP protein were run on an SDS-PAGE gel and transferred to a membrane. After renaturation of proteins, the membrane was incubated with recombinant human cGAS as a probe, which was detected using α-cGAS antibody. After stripping, the proteins on the membrane were detected using α-FLAG antibody. **(G)** Recombinant human cGAS-HA was mixed with recombinant FLAG-ORF9 or FLAG-GFP. Proteins were immunoprecipitated using α-HA and α-FLAG antibodies. Input, unbound and IP fractions were analysed by immunoblotting.

Panels (A) and (G) are representative of two independent experiments. Panels (B), (D), and (F) are representative of three independent experiments. Panel (C) is representative of two (HaCaT) and three (THP1) independent experiments.

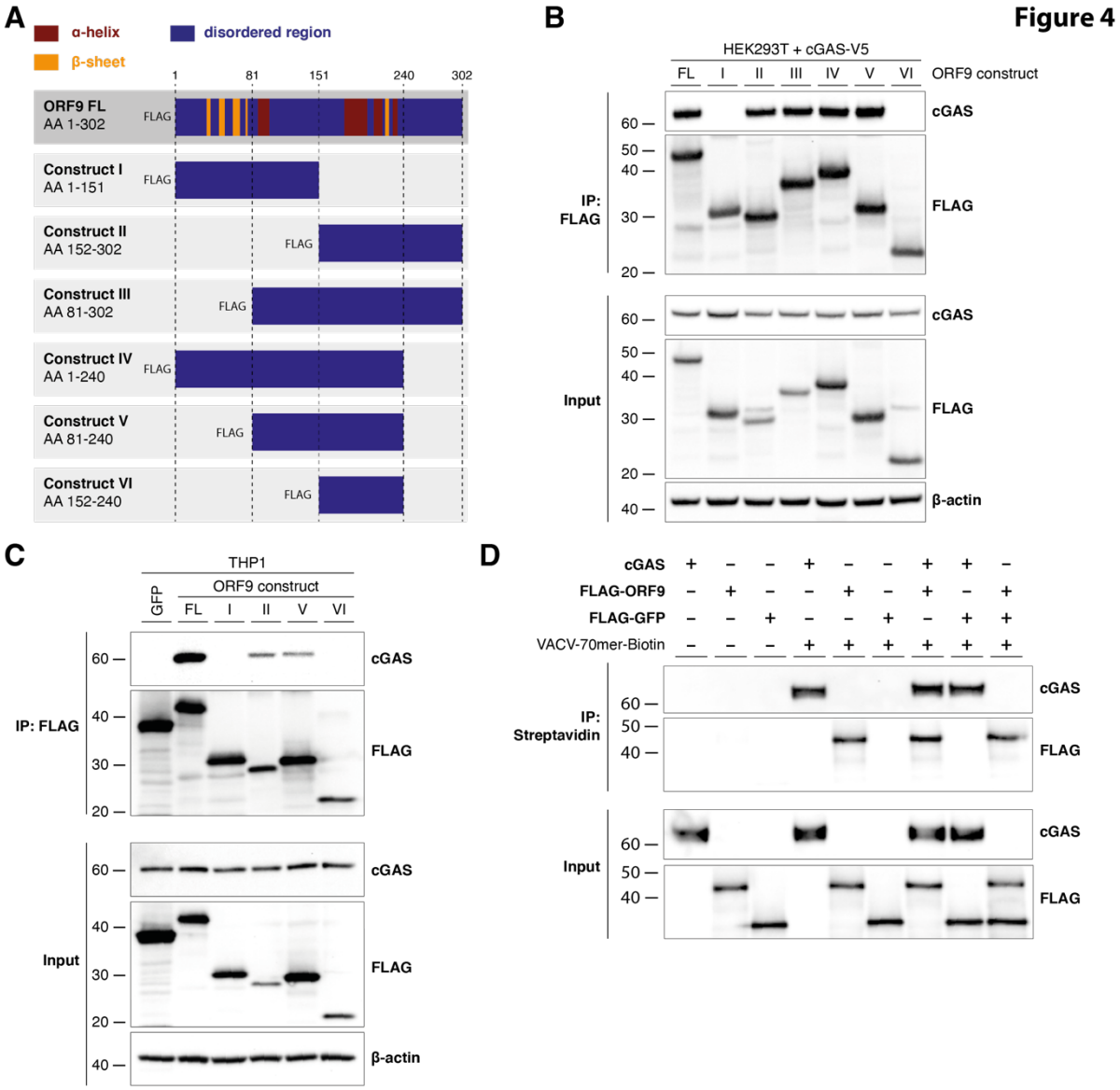

Figure 4. ORF9 binds DNA and interacts with cGAS *via* its central region.
(A) Schematic showing the ORF9 truncation mutants used in (B) and (C). Secondary structure features are based on predictions made using predictprotein.org (see methods). **(B)** HEK293T cells were transfected with human cGAS-V5 and full-length FLAG-ORF9, or different FLAG-tagged ORF9 truncation mutants. ORF9 constructs were immunoprecipitated using α-FLAG antibody. Input and IP fractions were subjected to immunoblotting using the indicated antibodies. **(C)** THP1 cells were stably transduced with FLAG-GFP, full-length FLAG-ORF9, or different FLAG-tagged ORF9 truncation mutants. ORF9 constructs were immunoprecipitated using α-FLAG antibody. Input and IP fractions were subjected to immunoblotting using the indicated antibodies. **(D)** Recombinant cGAS, FLAG-ORF9, FLAG-GFP, and biotinylated VACV-70mer dsDNA were incubated in the indicated combinations. Lysates were precipitated using streptavidin beads. Fractions were analysed by immunoblotting using the indicated antibodies.
Panel (B) is representative of two independent experiments. Panels (C) and (D) are from one experiment.

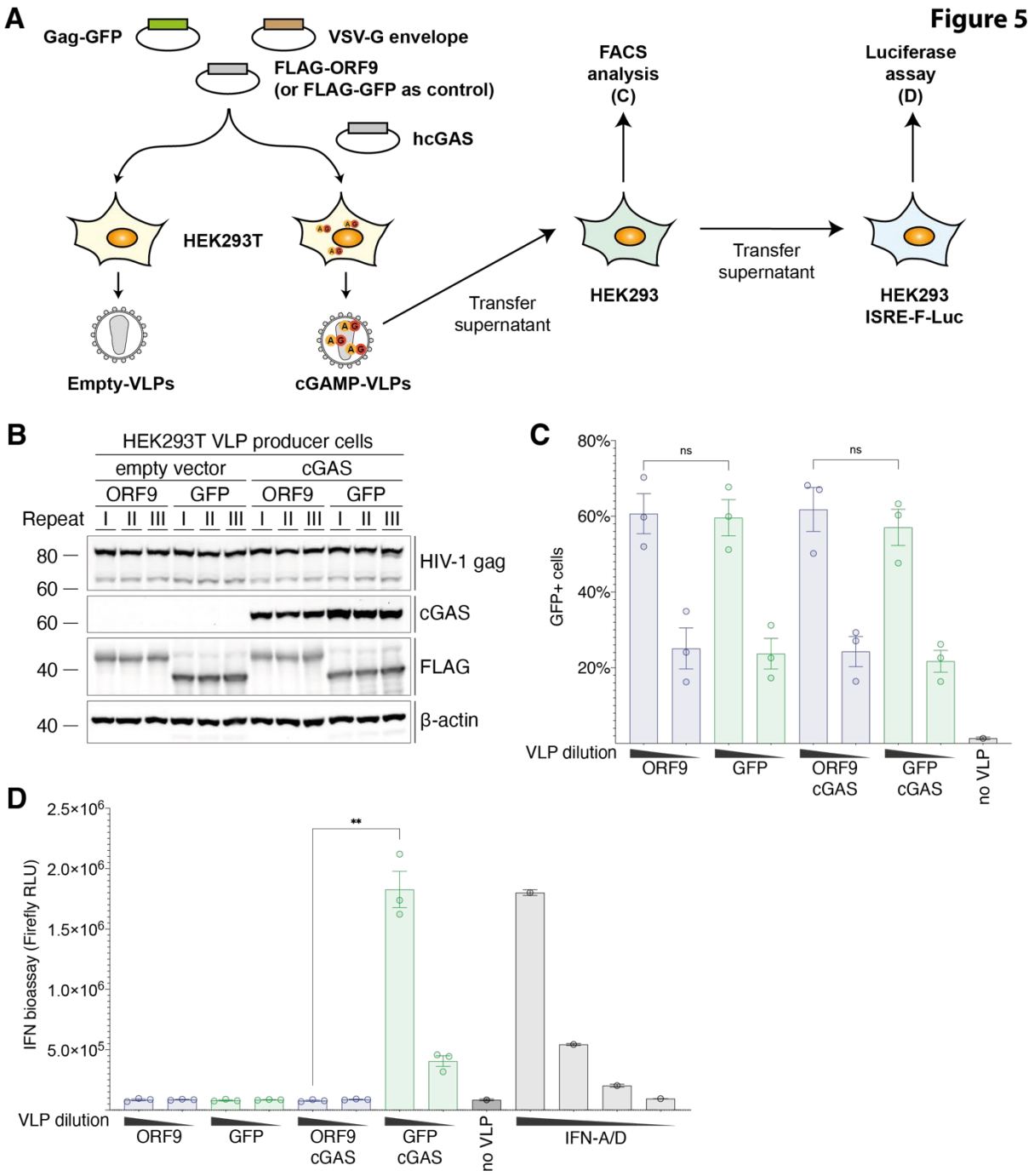

Figure 5. VZV ORF9 prevents cGAMP-loading of VLPs.

(A) Schematic of the experimental procedure. **(B)** HEK293T cells were transfected with plasmids encoding HIV-1 gag-GFP, VSV-G, FLAG-ORF9 or FLAG-GFP, and human cGAS or empty vector. Supernatants containing VLPs were harvested, and cells were lysed for immunoblotting using the indicated antibodies. **(C)** HEK293 cells were incubated with VLP containing supernatants (neat or diluted 1:2). The next day, cells were harvested and analysed by flow cytometry. The percentage of GFP^+ cells is shown. **(D)** HEK293 cell supernatants from (C) were added onto HEK293-ISRE-F-Luc cells. Recombinant IFN-A/D was used as a control (12.5, 6.25, 3.125, and 0 U/ml). After overnight incubation, firefly luciferase activity was determined.

The experiment was repeated three times. In panel (B), lysates from all three repeats were analysed. Panels (C) and (D) show pooled data (mean ± SEM). Statistical analysis: paired, two-tailed t-test, **=p<0.01, ns=not significant.

MATERIALS AND METHODS

Cells

All cells were cultured at 37°C and 5% CO_2 and checked regularly for mycoplasma contamination. Adherent cells were passaged using Trypsin-EDTA (0.25%) dissociation reagent (Gibco) at appropriate confluence. FCS was obtained from Sigma-Aldrich. HEK293 and HEK293T cells (gifts from Caetano Reis e Sousa, The Francis Crick Institute, UK) were maintained in DMEM (Sigma-Aldrich) containing 4.5 g/L glucose, supplemented with 10% (v/v) FCS and 2mM L-glutamine (Gibco) (DMEM complete). HEK293-ISRE-Firefly luciferase reporter cells (clone 3C11) were described previously (Bridgeman et al., 2015). HaCaT cells were a gift from Leonie Unterholzner (Lancaster University, UK) and were maintained in DMEM complete medium. MeWo cells were a gift from Graham Ogg (University of Oxford, UK) and were maintained in MEM supplemented with 10% (v/v) FCS, 2mM L-glutamine (Gibco), 1x Non-essential amino acids (Gibco), and 1mM sodium pyruvate (Gibco). THP1 Dual cells (WT, MyD88-KO, and IFNAR2-KO) were from Invivogen. cGAS-KO, STING-KO, and TBK1-KO THP1 cells were a gift from Soren Paludan (Aarhus University, Denmark) (Holm et al., 2016). MAVS-KO and IRF3-KO cells were generated on the THP1 Dual background as described below. All THP1 cell lines were maintained in RPMI (Sigma Aldrich) supplemented with 10% (v/v) FCS and 2mM L-glutamine (Gibco).

Viruses

VZV rOka (cosmid-derived recombinant pOka) was a gift from Jeffrey Cohen (NIH, Bethesda, USA) (Cohen and Seidel, 1993). The virus was maintained in monolayers of MeWo cells. In brief, monolayers of infected cells were monitored microscopically for cytopathic effect. Cells that showed high level of infection were detached and infected cells were mixed at appropriate ratios (1:2-1:4) with uninfected cells and re-plated. Aliquots of infected cells were cryopreserved in freezing medium (90% FCS, 10% DMSO), stored in liquid nitrogen, and thawed for experiments. $VZV^{ORF9\text{-}V5}$ is a recombinant virus, in which a C-terminal V5 tag was added to the coding sequence of ORF9. The virus was a kind gift from Catherine Sadzot (University of Liege, Belgium) (Riva et al., 2013).

Plasmids

The p125-Luc plasmid (*hIFNB1* promotor firefly luciferase) was a gift from T. Fujita (Kyoto University, Japan) (Yoneyama et al., 2004). pRL-TK was from Promega. RIG-I-CARD was a gift from Andreas Pichlmair (Technical University Munich, Germany). pCMV-VSV-G was a gift from Bob Weinberg (Addgene number 8454). The lentiviral packaging plasmid p8.91 was a gift from Greg Towers (University College London). pGag-eGFP was from the NIH AIDS reagent programme (number 11468). pX458/Ruby/MAVS was described previously (Hertzog et al., 2018). pCMV-3tag-KSHV-

ORF52 was a kind gift from Fanxiu Zhu (Florida State University, USA). pX458/Ruby/IRF3 was created as described for the MAVS-targeting plasmid. A sgRNA targeting exon 3 of the IRF3 locus was designed using the MIT algorithm (crispr.mit.edu) and cloned into the px458 vector. The pLenti6.3/EMCV-L-V5 plasmid was described previously (Hertzog et al., 2018).

Cloning

Mammalian expression plasmids for hcGAS and hSTING were created by PCR-amplification using THP1 cDNA and ligation into the gateway entry vector pCR8. Coding sequences were shuttled into expression vectors (pLenti6.3/C-V5, pcDNA3.2/C-FLAG, pcDNA3.2/C-HA) *via* Gateway recombination. Mammalian expression plasmids for eGFP (pLenti6.3/puro/N-FLAG, pDEST31/N-FLAG) were created in a similar way by PCR amplification from pGag-eGFP introducing a stop codon. VZV ORF9 expression plasmids (pLenti6.3/puro/N-FLAG, pDEST31/N-FLAG) were created by amplification of ORF9 with a stop codon and gateway recombination. Expression plasmids for ORF9 truncation mutants (pLenti6.3/puro/N-FLAG) were created by PCR amplification of the respective coding sequence with a start and stop codon. Bacterial expression vectors for FLAG-ORF9, FLAG-GFP, and hcGAS-HA were created by PCR-amplification of the coding sequences from existing plasmids and restriction enzyme cloning into pGEX6P1. pGEX6P1 and pGEX6P1-hcGAS were a kind gift from Martin Reijns (University of Edinburgh, UK). All primer sequences are listed in Table S1.

VACV 70mer-Biotin dsDNA

A 70bp immunostimulatory dsDNA fragment from VACV was described previously (Unterholzner et al., 2010). Two complementary oligos were synthesised (Sigma Aldrich) and combined at equal molar ratio. The solution was heated to 95°C and allowed to anneal by cooling to RT.
Forward sequence:
5'-ccatcagaaagaggtttaatatttttgtgagaccatcgaagagagaaagagataaaacttttttacgact-3'-TEG-Biotin
Reverse sequence:
5'- agtcgtaaaaaagttttatctctttctctcttcgatggtctcacaaaaa-tattaaacctctttctgatgg-3'

Antibodies

For immunoblot: beta-actin-HRP (AC-15, Sigma Aldrich), FLAG-HRP (clone M2, Sigma Aldrich), V5-HRP (R961-25, Invitrogen), RIG-I (Alme1, Calteg Medsystems), VZV gE/GI (MAB8612, GE Healthcare), VZV ORF62 (C05107MA, Meridian Life Science), pSTAT1 (Y701) (58D6, CellSignaling Technology), STAT1 (42H3, CellSignaling Technology), pSTAT2 (D3P2P, CellSignaling Technology), STAT2 (D9J7L, CellSignaling Technology), hcGAS (D1D3G, CellSignaling Technology), hSTING (D2P2F, CellSignaling Technology), MyD88 (D80F5, CellSignaling

Technology), TBK1 (D1B4, CellSignaling Technology), MAVS (ALX-210-929-C100, ENZO Life Science), IRF3 (D6I4C, CellSignaling Technology), VZV ORF9 (polyclonal rabbit serum, kind gift from Catherine Sadzot (University of Liege, Belgium) (Riva et al., 2013), donkey-anti-mouse-HRP (NA931, GE Healthcare), donkey-anti-rabbit-HRP (NA931, GE Healthcare). For IP: FLAG (clone M2, Sigma Aldrich, V5 (680602, Biolegend), HA (2-2.2.14, Invitrogen). For IF: V5-FITC (R963-25, Invitrogen), FLAG (D6W5B, CellSignaling Technology), goat-anti-rabbit-AF647 (A21246, Invitrogen). For FACS: VZV gE/gI (see above) was conjugated to FITC using FITC Conjugation Kit (Abcam).

VZV ORF Library

Primers for PCR amplification of individual VZV ORF sequences were designed based on an annotated VZV genome sequence (GenBank accession: AB097933.1). Forward primers included a Kozak sequence (GCCGCC), added before the start codon of an ORF. Reverse primers excluded the Stop codon to allow for addition of a C-terminal tag through the vector (see below). Primer sequences are listed in Table S2. The PCR template was generated by extracting RNA from VZV infected MeWo cells using QIAshredder (Qiagen) and RNeasy Mini Kit (Qiagen). The RNA was reverse transcribed into cDNA using SuperScript II Reverse Transcriptase (Invitrogen). For some ORFs, DNA from infected MeWo cells extracted with DNeasy Blood and Tissue Kit (Qiagen) served as the PCR template. PCR products were generated using Phusion High-Fidelity DNA Polymerase (New England Biolabs) or Herculase II Fusion DNA Polymerase (Agilent Technologies). PCR reactions were analysed by agarose gel electrophoresis and PCR products of the predicted size were extracted from the gel using QIAquick Gel Extraction Kit (Qiagen). Fragments were ligated into the pCR8/TOPO Gateway entry vector (Invitrogen). Plasmid DNA from single clones of transformed *E.coli* (New England Biolabs) was analysed for correct orientation of the insert by Sanger sequencing. Inserts were then shuttled into pLenti6.3/TO/V5-DEST (Invitrogen) using LR Clonase II Enzyme Mix (Invitrogen) for Gateway recombination. All clones with the pLenti6.3/TO/V5 backbone were propagated in recombination-deficient Stbl3 bacteria (Invitrogen).

Cloning of the entire coding sequence of ORF22 (8256 bp) was unsuccessful using various amplification and cloning technologies. Therefore, two Gateway entry vectors encoding individual segments within the ORF22 coding sequence (ORF22A: nt 2219-4029, ORF22B: nt 4012-6114, described previously (Uetz et al., 2006)) were used (kind gift from Jurgen Haas, University of Edinburgh, UK). Expression vectors with the pLenti6.3/TO/V5 backbone were generated as described above.

To validate expression, HEK293T were seeded at $5x10^5$ cells per well in 12-well plates. The next day, cells were transfected with 600ng VZV ORF or control expression plasmids using 3µl Lipofectamine 3000 (Invitrogen) per well. 24 hours later, cells were lysed in RIPA buffer (10mM TRIS-HCl pH8, 140mM NaCl, 1% Triton-X 100, 0.1% SDS, 0.1% sodium deoxycholate, 1mM EDTA, 0.5mM EGTA). Lysates were clarified by centrifugation and 30µg protein was subjected to immunoblotting.

IFN Reporter Assay

HEK293T cells were seeded at $3.5x10^4$ cells per well in 96-well plates. On the following day, cells were transfected with the following plasmids using Lipofectamine 2000 (Invitrogen): 20ng p125-F-Luc, 5ng pRL-TK, 1ng hcGAS, 25ng hSTING, and 50ng of a VZV ORF. Alternatively, cells were transfected with 5ng RIG-I-CARD plasmid instead of cGAS and STING plasmids. The next day, expression of firefly and renilla luciferases was assessed using Dual Luciferase assay system (Promega).

Lentivirus Production and Transduction

$1.2x10^7$ HEK293T cells were seeded in 15cm cell culture dishes. The next day, cells were transfected with 9µg lentiviral expression plasmids harbouring the gene of interest, 9µg p8.91 plasmid, and 3µg pVSV-G using Lipofectamine 2000. 16 hours later, medium was replaced with fresh growth medium. 24 hours later, lentivirus containing supernatant was harvested, clarified by centrifugation, and stored at 4°C. Cells were overlaid with fresh growth medium. 8 hours later, supernatants were harvested again and pooled with previous supernatants. After 16 hours, lentivirus containing supernatants were harvested for a third time. Pooled supernatants from all three harvests were filtered through a 0.45µm filter, aliquoted into cryovials and stored at -80°C. For transduction of cells, polybrene (Sigma Aldrich) was added to lentiviral supernatants to a final concentration of 8µg/ml. THP1 cells were pelleted and resuspended in lentiviral supernatant containing polybrene. The next day, cells were pelleted and resuspended in fresh growth medium. After overnight incubation, cells were once again pelleted and resuspended in growth medium containing 10µg/ml blasticidin or 1µg/ml puromycin (both Gibco) depending on which vector was used. Surviving cells were used for experiments.

cGAMP-loaded VLPs

Empty VLPs or VLPs which incorporated cGAMP were generated using a modified procedure based on a previously described method (Bridgeman et al., 2015). $1.4x10^6$ HEK293T cells were seeded per well in 6-well plates. The next day, cells were transfected with 2µg of plasmids pDEST31/FLAG-ORF9 or pDEST31/FLAG-GFP, 1µg pGag-eGFP (NIH AIDS reagent program), 500ng pVSV-G, and 1µg of pcDNA3.2/hcGAS or pcDNA3.2/empty-vector. VLPs were harvested as described above. At the end of VLP production, cells were lysed in RIPA buffer and analysed by immunoblotting.

$1.75x10^5$ HEK293 cells were seeded per well in 24-well plates. The next day, cells were overlaid with VLP solutions neat or 1:2 diluted in DMEM in the presence of 8µg/ml polybrene (Sigma Aldrich) in duplicate. 16 hours later, supernatants were used for IFN bioassay (see below). The cells were resuspended in PBS and stained with 1µg/ml DAPI (Sigma Aldrich) in PBS for 10min. Cells were washed, fixed with BD CellFix (BD) and analysed immediately on Attune NxT Acoustic Focusing Cytometer (Thermo

Fisher). Cells were gated on single, live events. A GFP^+ gate was set based on uninfected cells.

IFN Bioassay

Type I IFN in cell culture supernatants was measured using HEK293-ISRE-Firefly luciferase reporter cells (clone 3C11) as described previously (Bridgeman et al., 2015). $4x10^4$ 3C11 cells were seeded per well into 96-well plates in growth medium. The next day, test supernatants were clarified by centrifugation and overlaid onto 3C11 cells seeded before. A standard consisting of 2-fold dilutions of recombinant IFN-A/D (Sigma-Aldrich) was analysed in parallel. After overnight incubation reporter activation in 3C11 cells was assessed by measuring luciferase activity using ONE-Glo luciferase assay (Promega).

THP1 Knockout Cell Generation

For generation of knockout cells using CRISPR/Cas9 technology the pX458-mRuby plasmid encoding the Cas9 protein, the sgRNA, and mRuby was used (Hertzog et al., 2018). $1x10^7$ THP1 cells were transiently transfected with 50µg of respective pX458 plasmids using Lipofectamine LTX (Invitrogen) and incubated overnight. The next day cells were stained with 10µg/ml DAPI in PBS for 10min. After resuspension of cells in growth medium, live, mRuby-positive cells were FACS-sorted into eppendorf tubes containing growth medium with 20% FCS. The suspension of sorted cells was diluted with special growth medium (50% conditioned THP1 medium, 40% fresh RPMI with 10% FCS, 10% additional FCS) to one or three cells per 200µl. 200µl cell suspension were then dispensed into each well of a 96-well plate (one or three cells per well). The cells were incubated for several weeks until clones grew out.
The absence of the targeted protein in each clone was assessed by immunoblot analysis. For functional validation, $1.5x10^5$ cells were seeded per well into 96-well plates in growth medium containing 10ng/ml PMA (Sigma-Aldrich). The next day cells were transfected with 5ng IVT-RNA (Rehwinkel et al., 2010) or 15ng *E.coli* DNA (Invivogen) using Lipofectamine 2000 (Invitrogen). 24 hours later, IFN in supernatants was measured using the type I IFN bioassay. Knockout clones were further analysed for insertions and deletions in their genomic loci. *MAVS* and *IRF3* target regions were PCR-amplified using Herculase II Fusion DNA Polymerase. PCR amplicons were gel extracted (QIAquick Gel Extraction Kit) and sequenced by Sanger sequencing. Sequencing traces were analysed using the TIDE software (https://tide.nki.nl) (Brinkman et al., 2014).

VZV Flow Cytometry Infection Assay

Cells were washed in FACS tubes with PBS and incubated with LIVE/DEAD Fixable Violet Dead Cell Stain (Invitrogen) diluted 1:1000 in PBS for 30min at 4°C. Cells were washed in PBS and resuspended in 100µl FACS buffer (1% FCS, 2mM EDTA in PBS)

containing 1:500 FITC-coupled antibody against VZV gE/gI complex. Cells were incubated 30min at 4°C. After washing with PBS cells were resuspended in PBS and an equal volume of 8% methanol-free formaldehyde in PBS was added. Cells were fixed for 15min at room-temperature. Cells were washed with PBS, resuspended in FACS buffer, and analysed on a Attune NxT Acoustic Focusing Cytometer (Thermo Fisher).

THP1 VZV Infections

$6.125x10^6$ THP1 cells were seeded per well in 6-well plates in growth medium containing 10 ng/ml PMA (Sigma-Aldrich). As a control, $1.625x10^6$ MeWo cells were seeded in MEM. The next day cells were washed with PBS and overlaid with PBS containing CellTrace Far Red dye (Invitrogen) diluted 1:5,000. Cells were labelled for 15min at 37°C, an excess of growth medium was added and cells were incubated for another 5min. Meanwhile, aliquots of uninfected and VZV-infected MeWo cells were thawed, washed, and resuspended in MEM. Cells were counted and their concentration was adjusted to $6.25x10^5$ live cells per ml (for THP1 cells) or $1.25x10^5$ live cells per ml (for MeWo cells) with MEM. Medium was removed from labelled cells and cells were overlaid with 2ml MeWo -/+VZV cell suspension. Cells were incubated at 37°C for 1 hour. The cell suspension was removed, adherent cells were washed with PBS, overlaid with their respective growth medium and incubated for 48 hours. Supernatants were removed from cells, clarified by centrifugation and stored at -80°C. CXCL10 levels were determined using Human CXCL10/IP-10 Quantikine ELISA Kit (R&D Systems) according to manufacturer's instructions. Cells were washed with PBS and incubated with Trypsin-EDTA until they started to detach. Growth medium was added, cells were resuspended by gentle pipetting and transferred to FACS tubes on ice. 45% of cell suspension were transferred to eppendorf tubes on ice for extraction of RNA and generation of protein lysates, respectively. The cells in those eppendorf tubes were pelleted, washed with PBS, and then lysed either in RLT buffer and processed for RT-qPCR or lysed in RIPA buffer and processed for immunoblot analysis. Remaining cells in FACS tubes were used for analysis by flow cytometry.

Pulldowns

$1.4x10^7$ HEK293T cells were seeded in 15cm cell culture dishes. The next day, cells were transfected with 12.7µg of ORF9-V5, cGAS-FLAG, and STING-HA expression plasmids using Lipofectamine 2000. 16 hours later, cells were lysed in IP buffer (20mM TRIS-HCl pH7.4, 100mM NaCl, 1mM EDTA, 0.5% NP-40, Protease Inhibitor Cocktail (CellSignaling Technology)). After clarification, an aliquot was removed as input sample and the lysate was split into four equal volumes. Each aliquot was incubated with 50µl Dynabeads Protein G that were coated with 5µg α-V5, α-FLAG, α-HA, or control IgG antibody for 1 hour under rotation at 4°C. The supernatant was removed, an aliquot was stored as unbound fraction from each sample, and beads were washed three times in lysis buffer. Input, unbound, and bound fractions were subjected to immunoblotting. For pulldowns from stably transduced THP1 cells, cells were seeded

at $2x10^7$ per dish in 15cm cell-culture dishes in growth medium containing 10ng/ml PMA. Lysates were generated the next day and processed as described above. For pulldowns of recombinant proteins, 3µl recombinant cGAS-HA protein was mixed with 1.5µl FLAG-ORF9 or FLAG-GFP in IP buffer. IP was performed as described above. For pulldowns from VZV-infected cells, $2.2x10^7$ THP1 cells and $4x10^6$ HaCaT cells were seeded in 10cm dishes (in the presence of 10ng/ml PMA for THP1 cells). The next day cells were overlaid with $1.25x10^7$ MeWo cells infected with VZV or $VZV^{ORF9\text{-}V5}$ for 1 hour and afterwards washed with PBS. Lysates were generated 48 hours later as described above.

Far western

The experimental procedure for far western was based on a protocol previously described (Wu et al., 2007). 1.5µl FLAG-ORF9 protein or 1.5µl FLAG-GFP protein was subjected to SDS-PAGE and blotting as described for regular immunoblotting (see below). After transfer, the membrane was incubated for 30min at RT temperature in AC buffer (6M Guanidine HCl, 100mM NaCl, 20mM TRIS-HCl pH 7.6, 0.5mM EDTA, 10% glycerol, 0.1% Tween-20, 2% skim milk powder, 1mM DTT). The membrane was then incubated in AC buffers with decreasing concentrations of Guanidine HCl (3M, 1M, 0.1M) for 30min each. For the last incubation the membrane was transferred to 4°C and thereafter incubated in AC buffer free of Guanidine HCl overnight. The membrane was blocked for 1 hour in 5% milk powder in PBST (PBS with 0.05% Tween-20) and then incubated with 10µl recombinant cGAS per 5ml buffer as probe in 3% milk powder in PBST for 1 hour. Membranes were washed for 10min with PBST thrice and then incubated with α-cGAS antibody for 1 hour. After washing, membranes were incubated with appropriate secondary antibodies, washed again, and imaged. Hereafter, membranes were stripped and re-probed with α-FLAG antibody as described for conventional immunoblot.

Immunofluorescence

$1.75x10^5$ HEK293T cells were seeded onto-glass coverslips. The next day, cells were transfected with 250ng of cGAS-V5 or FLAG-ORF9 expression plasmid using 1.5µl Lipofectamine 3000 per well. Additional coverslips were co-transfected with both plasmids. 24 hours later cells were washed with PBS and fixed with 4% formaldehyde in cytoskeleton stabilisation buffer (CSB; 10mM KCl, 274mM NaCl, 8mM $NaHCO_3$, 0.8mM KH_2PO_4, 2.2mM Na_2HPO_4, 4mM $MgCl_2$, 10mM PIPES, 4mM EGTA, 11mM glucose) for 15min. Cells were washed and permeabilised with 0.1% Triton X-100 in CSB for 20min and incubated with 100mM glycine in CSB for 10min afterwards. Cells were washed with PBS four times and blocked using 1% BSA and 5% normal goat serum (Invitrogen) in PBS for 1 hour. Coverslips were incubated with primary antibodies in blocking solution for 3 hour at room temperature. Cells were washed three times with PBS and incubated with secondary antibodies in blocking solution for 1 hour. Coverslips were washed with PBS three times and mounted onto glass slides

using ProLong Diamond Antifade Mountant with DAPI (Invitrogen). Images were acquired using a Zeiss LSM780 confocal microscopy system (Zeiss).

Recombinant Protein Expression

BL21-pLysS-Rosetta *E.coli* (kind gift from Simon Davis, University of Oxford, UK) were transformed with bacterial expression vectors. A single colony or a glycerol stock from a single colony were used to inoculate a starter culture of 25ml LB-medium containing 34µg/ml Chloramphenicol and 100µg/ml Carbenicillin. A large 400ml LB culture was inoculated using the starter culture. OD600 was measured in intervals and, for VZV ORF9 and GFP, recombinant protein expression was induced by adding 0.1mM IPTG once OD reached 0.6. Bacteria were grown 3 hours at 37°C. For expression of recombinant cGAS and cGAS-HA, bacteria were grown to OD 0.8 and chilled to 18°C. Protein expression was induced by adding 0.4mM IPTG and bacteria were incubated for 16 hours at 18°C. For all proteins, bacteria were pelleted at 6,000g for 7min and the pellet was resuspended in 12ml lysis buffer (20mM TRIS pH7.4, 500mM NaCl, 0.5mM EDTA, 0.5mM EGTA, 0.5% NP40, 1:100 Protease Inhibitor Cocktail (CellSignaling Technology)). The suspension was sonicated on ice three times at 20% amplitude with 15 sec ON and 30 sec OFF (Branson Sonifier). Insoluble material was removed by centrifugation for 15min at 24,000g. In the meantime, 150µl Glutathione Sepharose beads (GE Healthcare) were prepared according to manufacturer's instructions. The beads were added to the clarified lysate and incubated under rotation for 4 hours at 4°C. The beads were pelleted by centrifugation at 500g and washed five times with lysis buffer. The beads were washed once in PreScission Cleavage buffer (50mM TRIS pH 7.5, 150mM, 1mM freshly added DTT) and resuspended in 500µl PreScission Cleavage buffer. After addition of 12µl PreScission Protease (GE Healthcare), the suspension was incubated under rotation for 3 hours at 4°C. The supernatant containing the recombinant protein was separated from beads and stored at -80°C. Aliquots from the various purification steps were analysed by SDS-PAGE and subsequent staining of the gel with EZBlue Gel Staining Reagent (Sigma Aldrich). Based on band intensities the protein concentrations were estimated to be ca. 1µg/µl for FLAG-ORF9 and FLAG-GFP, and ca. 0.5µg/µl for cGAS and cGAS-HA.

Immunoblotting

Protein concentrations in lysates were determined using Pierce BCA Protein Assay Kit (Thermo Scientific) and equalised by dilution of samples with lysis buffer. Subsequently, 4x NuPAGE LDS Sample Buffer (Invitrogen) was added and samples were incubated at 95°C for 10min. Samples were run on NuPAGE Novex 4-12% Bis-TRIS gels (Invitrogen) using NuPage MOPS-SDS running buffer (Invitrogen). Proteins were subsequently blotted onto PROTRAN Pure nitrocellulose membrane (PerkinElmer) using transfer buffer (25mM TRIS, 192mM glycine). Membranes were blocked with 5% skim milk powder (Sigma-Aldrich) in TBS containing 0.1% Tween-20 (5% milk TBS-T) for 1 hour at room temperature and were then incubated with primary antibodies in 5% milk TBS-T overnight at 4°C. Primary antibodies that bind to

phosphorylated residues were diluted in 5% BSA in TBS-T. Membranes were washed thrice with TBS-T and incubated with HRP-coupled secondary antibodies in 5% milk TBS-T for 1 hour at room temperature. After three further washes with TBS-T, proteins were detected using Western Lightning Plus-ECL (PerkinElmer) and the iBright FL1000 Imaging System (Thermo Fisher) or Amersham Hyperfilm MP (GE Healthcare). If needed, antibodies were stripped from the membrane with stripping buffer (200mM glycine, 0.1% SDS, 1% Tween-20, pH 2.2) for 20min at room temperature. Membranes were washed with TBS-T, blocked as described above and re-probed.

RT-qPCR

Cells were lysed in RLT Plus buffer and RNA was extracted using RNeasy Plus Mini Kit (Qiagen). The RNA was reverse transcribed using SuperScript IV Reverse Transcriptase (Invitrogen) and oligo-dT primers (Invitrogen). The qPCR reaction containing TaqMan Universal PCR Master Mix (Applied Biosystems) and TaqMan Primer/Probes was run on QuantStudio 7 Flex Real-Time PCR System (Thermo Fisher) with standard settings. Gene expression was analysed with the Ct method using *GAPDH* expression for normalisation. Taqman primer/probes used were: *GAPDH* (Hs02758991_g1), *IFNB1* (Hs02621180_s1), *IFI44* (Hs00951349_m1), and *IFNL1* (Hs00601677_g1).

Protein sequence analysis

The HSV-1 VP22 (PDB: 4XAL) and MHV68 ORF52 (PDB: 2OA5) crystal structures were used to graphically represent secondary structure features. For VZV ORF9 (UniProt accession Q4JQW6) and KSHV ORF52 (UniProt accession F5HBL8), structural features and sequence disorder was predicted by the PROFphd secondary structure prediction algorithm through submission of protein sequences to the predictprotein.org web interface (Yachdav et al., 2014).

Data Analysis and Software

Data were analysed using Excel for Mac (Microsoft) and GraphPad Prism 8 (GraphPad Software). SnapGene (GSL Biotech) and ApE (M. Wayne Davis, The University of Utah) were utilised for DNA sequence analysis to assist cloning. Statistical analysis is detailed in the figure legends and was performed using GraphPad Prism 8. Graphs and figures were created using GraphPad Prism 8 and Adobe Illustrator CC (Adobe Systems). Immunoblot images were processed using web-based iBright Image Analysis software (Thermo Fisher). Flow cytometry data was analysed using FlowJo (FlowJo, LLC). Fiji 2.0.0 software was used to process confocal microscopy images (Schindelin et al., 2012).

REFERENCES

Abendroth, A., Morrow, G., Cunningham, A.L., and Slobedman, B. (2001). Varicella-zoster virus infection of human dendritic cells and transmission to T cells: implications for virus dissemination in the host. J Virol *75*, 6183-6192.

Ablasser, A., and Chen, Z.J. (2019). cGAS in action: Expanding roles in immunity and inflammation. Science *363*, eaat8657.

Ablasser, A., Goldeck, M., Cavlar, T., Deimling, T., Witte, G., Röhl, I., Hopfner, K.-P., Ludwig, J., and Hornung, V. (2013). cGAS produces a 2′-5′-linked cyclic dinucleotide second messenger that activates STING. Nature *498*, 380-384.

Almine, J.F., O'Hare, C.A.J., Dunphy, G., Haga, I.R., Naik, R.J., Atrih, A., Connolly, D.J., Taylor, J., Kelsall, I.R., Bowie, A.G.*, et al.* (2017). IFI16 and cGAS cooperate in the activation of STING during DNA sensing in human keratinocytes. Nat Commun *8*, 679.

Andreeva, L., Hiller, B., Kostrewa, D., Lässig, C., de Oliveira Mann, C.C., Jan Drexler, D., Maiser, A., Gaidt, M., Leonhardt, H., Hornung, V.*, et al.* (2017). cGAS senses long and HMGB/TFAM-bound U-turn DNA by forming protein–DNA ladders. Nature *549*, 394-398.

Arvin, A.M., and Gilden, D. (2013). Varicella-Zoster Virus. In Virology, B.N. Fields, D.M. Knipe, and P.M. Howley, eds. (Philadelphia: Wolters Kluwer Health/Lippincott Williams & Wilkins), pp. 2015-2057.

Arvin, A.M., Koropchak, C.M., Williams, B.R.G., Grumet, F.C., and Foung, S.K.H. (1986). Early Immune Response in Healthy and Immunocompromised Subjects with Primary Varicella-Zoster Virus Infection. The Journal of Infectious Diseases *154*, 422-429.

Barrat, F.J., Elkon, K.B., and Fitzgerald, K.A. (2016). Importance of Nucleic Acid Recognition in Inflammation and Autoimmunity. Annu Rev Med *67*, 323-336.

Bridgeman, A., Maelfait, J., Davenne, T., Partridge, T., Peng, Y., Mayer, A., Dong, T., Kaever, V., Borrow, P., and Rehwinkel, J. (2015). Viruses transfer the antiviral second messenger cGAMP between cells. Science *349*, 1228-1232.

Brinkman, E.K., Chen, T., Amendola, M., and van Steensel, B. (2014). Easy quantitative assessment of genome editing by sequence trace decomposition. Nucleic Acids Res *42*, e168-e168.

Brito, A.F., and Pinney, J.W. (2018). Time-calibrated tree reconciliations reveal frequent losses, intrahost speciations, and host switches in the evolution of herpesviruses. Biorxiv, 418111.

Brubaker, S.W., Bonham, K.S., Zanoni, I., and Kagan, J.C. (2015). Innate immune pattern recognition: a cell biological perspective. Annu Rev Immunol *33*, 257-290.

Buchan, D.W.A., and Jones, D.T. (2019). The PSIPRED Protein Analysis Workbench: 20 years on. Nucleic Acids Res *47*, W402-W407.

Campbell, T.M., McSharry, B.P., Steain, M., Ashhurst, T.M., Slobedman, B., and Abendroth, A. (2018). Varicella zoster virus productively infects human natural killer cells and manipulates phenotype. PLoS Pathog *14*, e1006999.

Carter-Timofte, M.E., Paludan, S.R., and Mogensen, T.H. (2018). RNA Polymerase III as a Gatekeeper to Prevent Severe VZV Infections. Trends in Molecular Medicine *24*, 904-915.

Caunt, A.E., and Taylor-Robinson, D. (2009). Cell-free varicella-zoster virus in tissue culture. Epidemiol Infect *62*, 413-424.

Chauveau, L., Bridgeman, A., Tan, T.K., Beveridge, R., Frost, J., Pedroza-Pacheco, I., Partridge, T., Borrow, P., Drakesmith, H., Townsend, A.*, et al.* (2020). cGAMP loading enhances the immunogenicity of VLP vaccines. Biorxiv, 2020.2001.2003.893586.

Che, X., Oliver, S.L., Reichelt, M., Sommer, M.H., Haas, J., Rovis, T.L., and Arvin, A.M. (2013). ORF11 Protein Interacts with the ORF9 Essential Tegument Protein in Varicella-Zoster Virus Infection. J Virol *87*, 5106-5117.

Che, X., Reichelt, M., Sommer, M.H., Rajamani, J., Zerboni, L., and Arvin, A.M. (2008). Functions of the ORF9-to-ORF12 Gene Cluster in Varicella-Zoster Virus Replication and in the Pathogenesis of Skin Infection. J Virol *82*, 5825-5834.

Chen, J.J., Zhu, Z., Gershon, A.A., and Gershon, M.D. (2004). Mannose 6-Phosphate Receptor Dependence of Varicella Zoster Virus Infection In Vitro and in the Epidermis during Varicella and Zoster. Cell *119*, 915-926.

Cohen, J.I., and Seidel, K.E. (1993). Generation of varicella-zoster virus (VZV) and viral mutants from cosmid DNAs: VZV thymidylate synthetase is not essential for replication in vitro. Proc Natl Acad Sci USA *90*, 7376-7380.

Davison, A.J. (2002). Evolution of the herpesviruses. Vet Microbiol *86*, 69-88.

de Oliveira Mann, C.C., Orzalli, M.H., King, D.S., Kagan, J.C., Lee, A.S.Y., and Kranzusch, P.J. (2019). Modular Architecture of the STING C-Terminal Tail Allows Interferon and NF-kappaB Signaling Adaptation. Cell Rep *27*, 1165-1175 e1165.

Dempsey, A., and Bowie, A.G. (2015). Innate immune recognition of DNA: A recent history. Virology *479-480*, 146-152.

Diner, E.J., Burdette, D.L., Wilson, S.C., Monroe, K.M., Kellenberger, C.A., Hyodo, M., Hayakawa, Y., Hammond, M.C., and Vance, R.E. (2013). The Innate Immune DNA Sensor cGAS Produces a Noncanonical Cyclic Dinucleotide that Activates Human STING. Cell Rep *3*, 1355-1361.

Drayman, N., Patel, P., Vistain, L., and Tay, S. (2019). HSV-1 single-cell analysis reveals the activation of anti-viral and developmental programs in distinct sub-populations. Elife *8*, 2503.

Du, M., and Chen, Z.J. (2018). DNA-induced liquid phase condensation of cGAS activates innate immune signaling. Science *361*, 704-709.

1025 Fitzgerald, K.A., McWhirter, S.M., Faia, K.L., Rowe, D.C., Latz, E., Golenbock, D.T.,
1026 Coyle, A.J., Liao, S.M., and Maniatis, T. (2003). IKKepsilon and TBK1 are essential
1027 components of the IRF3 signaling pathway. Nat Immunol *4*, 491-496.

1028 Freundt, E.C., Drappier, M., and Michiels, T. (2018). Innate Immune Detection of
1029 Cardioviruses and Viral Disruption of Interferon Signaling. Front Microbiol *9*, 867.

1030 Gerada, C., Campbell, T.M., Kennedy, J.J., McSharry, B.P., Steain, M., Slobedman,
1031 B., and Abendroth, A. (2020). Manipulation of the Innate Immune Response by
1032 Varicella Zoster Virus. Front Immunol *11*, 1.

1033 Haberthur, K., and Messaoudi, I. (2013). Animal Models of Varicella Zoster Virus
1034 Infection. Pathogens *2*, 364-382.

1035 Harding, S.M., Benci, J.L., Irianto, J., Discher, D.E., Minn, A.J., and Greenberg, R.A.
1036 (2017). Mitotic progression following DNA damage enables pattern recognition within
1037 micronuclei. Nature *548*, 466-470.

1038 Hartmann, G. (2017). Nucleic Acid Immunity. Adv Immunol *133*, 121-169.

1039 Hertzog, J., Dias Junior, A.G., Rigby, R.E., Donald, C.L., Mayer, A., Sezgin, E.,
1040 Song, C., Jin, B., Hublitz, P., Eggeling, C*., et al.* (2018). Infection with a Brazilian
1041 isolate of Zika virus generates RIG-I stimulatory RNA and the viral NS5 protein
1042 blocks type I IFN induction and signaling. Eur J Immunol *48*, 1120-1136.

1043 Hew, K., Dahlroth, S.-L., Nordlund, P., Cornvik, T., and Pan, L.X. (2015). VP22 core
1044 domain from Herpes simplex virus 1 reveals a surprising structural conservation in
1045 both the Alpha- and Gammaherpesvirinae subfamilies. Journal of General Virology
1046 *96*, 1436-1445.

1047 Holm, C.K., Rahbek, S.H., Gad, H.H., Bak, R.O., Jakobsen, M.R., Jiang, Z., Hansen,
1048 A.L., Jensen, S.K., Sun, C., Thomsen, M.K*., et al.* (2016). Influenza A virus targets a
1049 cGAS-independent STING pathway that controls enveloped RNA viruses. Nat
1050 Commun *7*, 10680.

1051 Horan, K.A., Hansen, K., Jakobsen, M.R., Holm, C.K., Soby, S., Unterholzner, L.,
1052 Thompson, M., West, J.A., Iversen, M.B., Rasmussen, S.B*., et al.* (2013).
1053 Proteasomal degradation of herpes simplex virus capsids in macrophages releases
1054 DNA to the cytosol for recognition by DNA sensors. J Immunol *190*, 2311-2319.

1055 Hu, S., Sun, H., Yin, L., Li, J., Mei, S., Xu, F., Wu, C., Liu, X., Zhao, F., Zhang, D*., et*
1056 *al.* (2019). PKR-dependent cytosolic cGAS foci are necessary for intracellular DNA
1057 sensing. Science Signaling *12*, eaav7934.

1058 Huang, J., You, H., Su, C., Li, Y., Chen, S., and Zheng, C. (2018). Herpes Simplex
1059 Virus 1 Tegument Protein VP22 Abrogates cGAS/STING-Mediated Antiviral Innate
1060 Immunity. J Virol *92*, 783.

1061 Ishikawa, H., Ma, Z., and Barber, G.N. (2009). STING regulates intracellular DNA-
1062 mediated, type I interferon-dependent innate immunity. Nature *461*, 788-792.

1063 Kennedy, J.J., Steain, M., Slobedman, B., and Abendroth, A. (2019). Infection and
1064 Functional Modulation of Human Monocytes and Macrophages by Varicella-Zoster
1065 Virus. J Virol *93*, 10980.

1066 Kim, J.-A., Park, S.-K., Seo, S.-w., Lee, C.H., and Shin, O.S. (2017). STING Is
1067 Involved in Antiviral Immune Response against VZV Infection via the Induction of
1068 Type I and III IFN Pathways. Journal of Investigative Dermatology *137*, 2101-2109.

1069 Kranzusch, P.J., Wilson, S.C., Lee, A.S.Y., Berger, J.M., Doudna, J.A., and Vance,
1070 R.E. (2015). Ancient Origin of cGAS-STING Reveals Mechanism of Universal 2′,3′
1071 cGAMP Signaling. Molecular Cell *59*, 891-903.

1072 Ku, C.-C., Chang, Y.-H., Chien, Y., and Lee, T.-L. (2016). Type I interferon inhibits
1073 varicella-zoster virus replication by interfering with the dynamic interaction between
1074 mediator and IE62 within replication compartments. Cell Biosci *6*, 519.

1075 Lebrun, M., Lambert, J., Riva, L., Thelen, N., Rambout, X., Blondeau, C., Thiry, M.,
1076 Snoeck, R., Twizere, J.-C., Dequiedt, F.*, et al.* (2018). Varicella-Zoster Virus ORF9p
1077 Binding to Cellular Adaptor Protein Complex 1 Is Important for Viral Infectivity. J Virol
1078 *92*, 222.

1079 Li, X., Shu, C., Yi, G., Chaton, C.T., Shelton, C.L., Diao, J., Zuo, X., Kao, C.C., Herr,
1080 A.B., and Li, P. (2013). Cyclic GMP-AMP Synthase Is Activated by Double-Stranded
1081 DNA-Induced Oligomerization. Immunity *39*, 1019-1031.

1082 Liu, S., Cai, X., Wu, J., Cong, Q., Chen, X., Li, T., Du, F., Ren, J., Wu, Y.T., Grishin,
1083 N.V.*, et al.* (2015). Phosphorylation of innate immune adaptor proteins MAVS,
1084 STING, and TRIF induces IRF3 activation. Science *347*, aaa2630.

1085 Luecke, S., Holleufer, A., Christensen, M.H., Jonsson, K.L., Boni, G.A., Sorensen,
1086 L.K., Johannsen, M., Jakobsen, M.R., Hartmann, R., and Paludan, S.R. (2017).
1087 cGAS is activated by DNA in a length-dependent manner. EMBO Rep *18*, 1707-
1088 1715.

1089 Lum, K.K., Song, B., Federspiel, J.D., Diner, B.A., Howard, T., and Cristea, I.M.
1090 (2018). Interactome and Proteome Dynamics Uncover Immune Modulatory
1091 Associations of the Pathogen Sensing Factor cGAS. Cell Syst *7*, 627-642.e626.

1092 Mackenzie, K.J., Carroll, P., Martin, C.-A., Murina, O., Fluteau, A., Simpson, D.J.,
1093 Olova, N., Sutcliffe, H., Rainger, J.K., Leitch, A.*, et al.* (2017). cGAS surveillance of
1094 micronuclei links genome instability to innate immunity. Nature *548*, 461-465.

1095 Mainka, C., Fuss, B., Geiger, H., Höfelmayr, H., and Wolff, M.H. (1998).
1096 Characterization of viremia at different stages of varicella-zoster virus infection. J
1097 Med Virol *56*, 91-98.

1098 McGeoch, D.J., Cook, S., Dolan, A., Jamieson, F.E., and Telford, E.A.R. (1995).
1099 Molecular Phylogeny and Evolutionary Timescale for the Family of Mammalian
1100 Herpesviruses. Journal of Molecular Biology *247*, 443-458.

1101 McNab, F., Mayer-Barber, K., Sher, A., Wack, A., and O'Garra, A. (2015). Type I
1102 interferons in infectious disease. Nat Rev Immunol *15*, 87-103.

1103 Mo, C., Lee, J., Sommer, M.H., and Arvin, A.M. (2003). Varicella-zoster virus
1104 infection facilitates VZV glycoprotein E trafficking to the membrane surface of
1105 melanoma cells. J Med Virol *70*, S56-S58.

1106 Morrow, G., Slobedman, B., Cunningham, A.L., and Abendroth, A. (2003). Varicella-
1107 Zoster Virus Productively Infects Mature Dendritic Cells and Alters Their Immune
1108 Function. J Virol *77*, 4950-4959.

1109 Nagel, M.A., and Gilden, D. (2014). Neurological complications of varicella zoster
1110 virus reactivation. Current Opinion in Neurology *27*, 356-360.

1111 Nour, A.M., Reichelt, M., Ku, C.-C., Ho, M.Y., Heineman, T.C., and Arvin, A.M.
1112 (2011). Varicella-Zoster Virus Infection Triggers Formation of an Interleukin-1β (IL-
1113 1β)-processing Inflammasome Complex. J Biol Chem *286*, 17921-17933.

1114 Radtke, K., Döhner, K., and Sodeik, B. (2006). Viral interactions with the
1115 cytoskeleton: a hitchhiker's guide to the cell. Cell Microbiol *8*, 387-400.

1116 Rehwinkel, J., Tan, C.P., Goubau, D., Schulz, O., Pichlmair, A., Bier, K., Robb, N.,
1117 Vreede, F., Barclay, W., Fodor, E.*, et al.* (2010). RIG-I Detects Viral Genomic RNA
1118 during Negative-Strand RNA Virus Infection. Cell *140*, 397-408.

1119 Riva, L., Thiry, M., Bontems, S., Joris, A., Piette, J., Lebrun, M., and Sadzot-Delvaux,
1120 C. (2013). ORF9p Phosphorylation by ORF47p Is Crucial for the Formation and
1121 Egress of Varicella-Zoster Virus Viral Particles. J Virol *87*, 2868-2881.

1122 Riva, L., Thiry, M., Lebrun, M., L'Homme, L., Piette, J., and Sadzot-Delvaux, C.
1123 (2015). Deletion of the ORF9p Acidic Cluster Impairs the Nuclear Egress of Varicella-
1124 Zoster Virus Capsids. J Virol *89*, 2436-2441.

1125 Schindelin, J., Arganda-Carreras, I., Frise, E., Kaynig, V., Longair, M., Pietzsch, T.,
1126 Preibisch, S., Rueden, C., Saalfeld, S., Schmid, B.*, et al.* (2012). Fiji: an open-source
1127 platform for biological-image analysis. Nat Methods *9*, 676-682.

1128 Schoggins, J.W. (2019). Interferon-Stimulated Genes: What Do They All Do? Annu
1129 Rev Virol *6*, 567-584.

1130 Schoggins, J.W., Wilson, S.J., Panis, M., Murphy, M.Y., Jones, C.T., Bieniasz, P.,
1131 and Rice, C.M. (2011). A diverse range of gene products are effectors of the type I
1132 interferon antiviral response. Nature *472*, 481-485.

1133 Sen, N., Sommer, M., Che, X., White, K., Ruyechan, W.T., and Arvin, A.M. (2010).
1134 Varicella-Zoster Virus Immediate-Early Protein 62 Blocks Interferon Regulatory
1135 Factor 3 (IRF3) Phosphorylation at Key Serine Residues: a Novel Mechanism of
1136 IRF3 Inhibition among Herpesviruses. J Virol *84*, 9240-9253.

1137 Shakya, A.K., O'Callaghan, D.J., and Kim, S.K. (2019). Interferon Gamma Inhibits
1138 Varicella-Zoster Virus Replication in a Cell Line-Dependent Manner. J Virol *93*, 3904.

1139 Sharma, S., tenOever, B.R., Grandvaux, N., Zhou, G.P., Lin, R., and Hiscott, J.
1140 (2003). Triggering the interferon antiviral response through an IKK-related pathway.
1141 Science *300*, 1148-1151.

1142 Smith, G.L., Talbot-Cooper, C., and Lu, Y. (2018). Chapter Fourteen - How Does
1143 Vaccinia Virus Interfere With Interferon? In Advances in Virus Research, M. Kielian,
1144 T.C. Mettenleiter, and M.J. Roossinck, eds. (Academic Press), pp. 355-378.

1145 Stempel, M., Chan, B., and Brinkmann, M.M. (2019). Coevolution pays off:
1146 Herpesviruses have the license to escape the DNA sensing pathway. Med Microbiol
1147 Immunol *208*, 495-512.

1148 Sun, L., Wu, J., Du, F., Chen, X., and Chen, Z.J. (2013). Cyclic GMP-AMP Synthase
1149 Is a Cytosolic DNA Sensor That Activates the Type I Interferon Pathway. Science
1150 *339*, 786-791.

1151 Tischer, B.K., Kaufer, B.B., Sommer, M., Wussow, F., Arvin, A.M., and Osterrieder,
1152 N. (2007). A Self-Excisable Infectious Bacterial Artificial Chromosome Clone of
1153 Varicella-Zoster Virus Allows Analysis of the Essential Tegument Protein Encoded by
1154 ORF9. J Virol *81*, 13200-13208.

1155 Torigo, S., Ihara, T., and Kamiya, H. (2000). IL-12, IFN-gamma, and TNF-alpha
1156 released from mononuclear cells inhibit the spread of varicella-zoster virus at an
1157 early stage of varicella. Microbiol Immunol *44*, 1027-1031.

1158 Uetz, P., Dong, Y.-A., Zeretzke, C., Atzler, C., Baiker, A., Berger, B., Rajagopala,
1159 S.V., Roupelieva, M., Rose, D., Fossum, E.*, et al.* (2006). Herpesviral Protein
1160 Networks and Their Interaction with the Human Proteome. Science *311*, 239.

1161 Unterholzner, L., Keating, S.E., Baran, M., Horan, K.A., Jensen, S.B., Sharma, S.,
1162 Sirois, C.M., Jin, T., Latz, E., Xiao, T.S.*, et al.* (2010). IFI16 is an innate immune
1163 sensor for intracellular DNA. Nat Immunol *11*, 997-1004.

1164 Wang, J.P., Kurt-Jones, E.A., Shin, O.S., Manchak, M.D., Levin, M.J., and Finberg,
1165 R.W. (2005). Varicella-Zoster Virus Activates Inflammatory Cytokines in Human
1166 Monocytes and Macrophages via Toll-Like Receptor 2. J Virol *79*, 12658-12666.

1167 West, A.P., Khoury-Hanold, W., Staron, M., Tal, M.C., Pineda, C.M., Lang, S.M.,
1168 Bestwick, M., Duguay, B.A., Raimundo, N., MacDuff, D.A.*, et al.* (2015).
1169 Mitochondrial DNA stress primes the antiviral innate immune response. Nature *520*,
1170 553-557.

1171 WHO (2014). Varicella and herpes zoster vaccines: WHO position paper, June 2014.
1172 Weekly epidemiological record *25*, 265-288.

1173 Wu, J., Sun, L., Chen, X., Du, F., Shi, H., Chen, C., and Chen, Z.J. (2013). Cyclic
1174 GMP-AMP Is an Endogenous Second Messenger in Innate Immune Signaling by
1175 Cytosolic DNA. Science *339*, 826.

1176 Wu, J.J., Li, W., Shao, Y., Avey, D., Fu, B., Gillen, J., Hand, T., Ma, S., Liu, X., Miley,
1177 W.*, et al.* (2015). Inhibition of cGAS DNA Sensing by a Herpesvirus Virion Protein.
1178 Cell Host Microbe *18*, 333-344.

1179 Wu, Y., Li, Q., and Chen, X.-Z. (2007). Detecting protein–protein interactions by far
1180 western blotting. Nat Protoc *2*, 3278-3284.

1181 Yachdav, G., Kloppmann, E., Kajan, L., Hecht, M., Goldberg, T., Hamp, T.,
1182 Honigschmid, P., Schafferhans, A., Roos, M., Bernhofer, M.*, et al.* (2014).
1183 PredictProtein-an open resource for online prediction of protein structural and
1184 functional features. Nucleic Acids Research *42*, W337-W343.

1185 Yoneyama, M., Kikuchi, M., Natsukawa, T., Shinobu, N., Imaizumi, T., Miyagishi, M.,
1186 Taira, K., Akira, S., and Fujita, T. (2004). The RNA helicase RIG-I has an essential
1187 function in double-stranded RNA-induced innate antiviral responses. Nat Immunol *5*,
1188 730-737.

1189 Yu, H.-R., Huang, H.-C., Kuo, H.-C., Sheen, J.-M., Ou, C.-Y., Hsu, T.-Y., and Yang,
1190 K.D. (2011). IFN-α production by human mononuclear cells infected with varicella-
1191 zoster virus through TLR9-dependent and -independent pathways. Cell Mol Immunol
1192 *8*, 181-188.

1193 Zerboni, L., Sen, N., Oliver, S.L., and Arvin, A.M. (2014). Molecular mechanisms of
1194 varicella zoster virus pathogenesis. Nat Rev Microbiol *12*, 197-210.

1195 Zhang, C., Shang, G., Gui, X., Zhang, X., Bai, X.-c., and Chen, Z.J. (2019). Structural
1196 basis of STING binding with and phosphorylation by TBK1. Nature *567*, 394-398.

1197 Zhang, X., Shi, H., Wu, J., Zhang, X., Sun, L., Chen, C., and Chen, Z.J. (2013).
1198 Cyclic GMP-AMP Containing Mixed Phosphodiester Linkages Is An Endogenous
1199 High-Affinity Ligand for STING. Molecular Cell *51*, 226-235.

1200 Zhang, X., Wu, J., Du, F., Xu, H., Sun, L., Chen, Z., Brautigam, C.A., Zhang, X., and
1201 Chen, Z.J. (2014). The Cytosolic DNA Sensor cGAS Forms an Oligomeric Complex
1202 with DNA and Undergoes Switch-like Conformational Changes in the Activation
1203 Loop. Cell Rep *6*, 421-430.

1204 Zhou, W., Whiteley, A.T., de Oliveira Mann, C.C., Morehouse, B.R., Nowak, R.P.,
1205 Fischer, E.S., Gray, N.S., Mekalanos, J.J., and Kranzusch, P.J. (2018). Structure of
1206 the Human cGAS–DNA Complex Reveals Enhanced Control of Immune
1207 Surveillance. Cell *174*, 300-311.e311.

1208 Zhu, H., Zheng, C., Xing, J., Wang, S., Li, S., Lin, R., and Mossman, K.L. (2011).
1209 Varicella-Zoster Virus Immediate-Early Protein ORF61 Abrogates the IRF3-Mediated
1210 Innate Immune Response through Degradation of Activated IRF3. J Virol *85*, 11079-
1211 11089.
1212